nature communications

Article

https://doi.org/10.1038/s41467-025-62632-x

# A mucosal vaccine prevents eosinophilic allergic airway inflammation by modulating immune responses to allergens in a murine model of airway disease

Received: 14 June 2024

Accepted: 25 July 2025

Published online: 03 August 2025

Check for updates

Carmen Sevilla-Ortega[1,2], Alba Angelina[1], Leticia Martín-Cruz[1,3], Mario Pérez-Diego[1], Angel Maldonado[1], Begoña Lavín[1], Beatriz Marcos-Ramiro[1], Luis Pérez de Llano[4], Auba Gayá[5], Francisco X. Real[5,6,7], Laura Conejero[2], José Luis Subiza[2] & Oscar Palomares[1]

Allergic sensitization and viral infections are risk factors for asthma development and progression. Sublingual vaccination with MV130, a whole heat-inactivated polybacterial preparation, protects against viral infections, but its impact on allergic sensitization and asthma development remains unknown. Here we show MV130 prevents house dust mite (HDM)-induced local type 2 immune responses and associated eosinophilic airway inflammation, conferring protection up to 9 weeks after vaccination. MV130 reduces pathophysiological and clinical asthma features in an in vivo experimental mouse model of HDM-induced allergic eosinophilic asthma, restoring normal airway functionality. MV130 impairs allergen-specific IgE sensitization and systemic type 2 inflammation endorsing type 1 and IL-10 responses. In human DCs, MV130 induces a transcriptomic and metabolic reprogramming, and restores non-pathological immune responses to allergens in healthy and asthmatic donors. Additionally, the adoptive transfer of MV130-stimulated BMDCs was sufficient to reproduce the protective features of the vaccine administration in vivo. Collectively, we show MV130 reduces allergic sensitization and eosinophilic asthma. Our findings support the exploration of mucosal interventions aimed at reducing the risk of allergen-induced asthma development.

Asthma is one of the most common chronic inflammatory disorders of the airways affecting children and adults with significant socio-economic burden[1,2]. It is characterized by variable and recurring symptoms (reversible airflow obstruction, wheezing, cough, and chest tightness), bronchial hyperresponsiveness (BHR) and chronic airway inflammation[3,4]. Asthma is a complex syndrome encompassing different phenotypes/endotypes that can be broadly stratified as type 2 (T2) or non-T2 immune-mediated according to T2 biomarkers and clinical

[1]Department of Biochemistry and Molecular Biology, School of Chemistry, Complutense University of Madrid, Madrid, Spain. [2]Inmunotek, Alcalá de Henares, Madrid, Spain. [3]Department of Biochemistry and Molecular Biology, School of Pharmacy, Complutense University of Madrid, Madrid, Spain. [4]Pneumology Service, Lucus Augusti University Hospital, EOXI Lugo, Monforte, Cervo, Lugo, Spain. [5]Epithelial Carcinogenesis Group, Centro Nacional de Investigaciones Oncológicas (CNIO), Madrid, Spain. [6]Centro de Investigación Biomédica en Red Cáncer, Madrid, Spain. [7]Departament de Medicina i Ciències de la Vida, Universitat Pompeu Fabra, Barcelona, Spain. e-mail: oscar.palomares@quim.ucm.es

features[3,5,6]. Allergic eosinophilic asthma is one of the most common T2 asthma pheno-endotype[3,4,7]. Upon encounter with allergens and environmental insults, bronchial epithelial cells produce alarmins (TSLP, IL-33 or IL-25)[8] that activate dendritic cells (DCs) and type 2 innate lymphoid cells (ILC2s), leading to allergic sensitization and T2 inflammatory responses characterized by high levels of serum allergen-specific IgE and increased numbers of allergen-specific Th2 and ILC2s in lungs and peripheral blood[4]. Activated allergen-specific Th2 cells and ILC2s produce large amounts of T2 cytokines (IL-4, IL-5, IL-9 and IL-13) contributing to eosinophilia, BHR, mucus production and IgE levels as the key pathophysiological features linked to the clinical signs and symptoms[3,4,9].

Compelling experimental evidence demonstrated that allergic sensitization and recurrent viral infections represent two main risk factors for asthma development and progression to difficult-to-treat and severe asthma[10,11]. Therapeutic strategies aimed at reducing viral infections and impairing allergic sensitization have been pointed out as promising alternatives to prevent asthma onset and severity[12]. In this regard, polybacterial preparations (PBPs), consisting of either bacterial lysates or whole heat-inactivated bacterial formulations, have demonstrated capacity to prevent recurrent respiratory viral infections in children by different ways of action[13–15]. In addition, PBPs, specific bacterial species or microbial-derived products, might well represent potential alternative treatments for allergic airway inflammation[16–19].

MV130 is a whole heat-inactivated PBP consisting of 90% of Gram positive (V102 *Staphylococcus aureus* (15%), V101 *S. epidermidis* (15%) and V104 *Streptococcus pneumoniae* (60%)) and 10% of Gram negative (V113 *Klebsiella pneumoniae* (4%), V105 *Moraxella catarrhalis* (3%) and V103 *Haemophilus influenzae* (3%)) bacteria[20]. MV130 acts on DCs of patients suffering recurrent respiratory tract infections enhancing their capacity to generate Th1, Th17 and IL-10-producing T cells against both related and unrelated antigens[20]. A phase III clinical trial showed that sublingual MV130 is safe and prevents recurrent wheezing in children conferring protection for at least 6 months after treatment discontinuation, thus pointing out to long-lasting innate trained immunity (TI) mechanisms[14]. Supporting these data, in vivo mouse models showed that MV130 protects against viral infections by TI mechanisms inducing metabolic and epigenetic reprogramming of innate cells and hematopoietic precursors[21]. These data convincingly demonstrated that MV130 mucosal vaccination induces TI and protects against recurrent viral infections. Therefore, MV130 falls within the concept of Trained Immunity-based Vaccine (TIbV), a new generation of vaccines that have the ability to induce non-specific responses to a variety of stimuli, including pathogens such as viruses, in addition to their nominal bacterial antigens[22]. MV130 may have an indirect effect on allergic inflammation by conferring protection against respiratory viruses[23,24]. On the other hand, it could also have a direct effect on such inflammation, as has been suggested for other bacterial products[18,19]. However, the potential capacity of MV130 to prevent allergic sensitization and eosinophilic airway inflammation as well as the underlying mechanisms remains elusive. Herein, we show that MV130 prevents house dust mite (HDM)-induced eosinophilic allergic airway inflammation and all the associated asthma features in an in vivo experimental mouse model, conferring protection up to 9 weeks upon treatment discontinuation. MV130 protects from the induction of type 2 innate and adaptive immune responses to allergens by impairing HDM-induced Th2 cells and ILC2s, thus blocking the recruitment of inflammatory eosinophils (iEos) without affecting homoeostatic resident eosinophils (rEos). MV130 also impairs IgE sensitization and systemic T2 responses without altering type 1 and IL-10 homoeostatic responses. In human DCs from healthy donors, MV130 inhibits their capacity to polarize HDM-induced Th2 responses and enhances Th1 and IL-10-producing T cells. Mechanistically, MV130 induces transcriptional and metabolic reprogramming in human DCs characterized by the activation of TNF-α-, IFN-γ-, IL-6- and IL-10-mediated pathways connected to increased glycolysis and reduced oxidative phosphorylation (OXPHOS), which might well be involved in the modulation of immune responses to allergens. Adoptive transfer of MV130-stimulated murine bone marrow-derived DCs (BMDCs) prior to in vivo HDM exposure impaired allergic sensitization and local airway inflammation through mechanisms associated with TLRs-mediated signalling pathways.

## Results

### MV130 impairs asthma immunopathology in a murine model of airway disease

To assess the in vivo capacity of MV130 to impair allergic sensitization and subsequent eosinophilic airway inflammation, we initially used a conventional experimental mouse model of HDM-induced allergic eosinophilic asthma (Fig. 1a)[25]. Mice were intranasally (i.n.) sensitized on day 1 and challenged afterwards during 5 consecutive days (days 8–12) with HDM allergen extracts. Mice were i.n. treated either with MV130 (HDM + MV130 group) or vehicle (HDM group) for 3 consecutive days (days 2–4) prior to allergen challenge (Fig. 1a). Non-sensitized mice receiving only PBS (PBS group) or receiving MV130 (days 2–4) alone without allergen sensitization/challenge (MV130 group) were used as controls (Fig. 1a). The HDM + MV130 group displayed a significant reduction of serum total IgE accompanied by a significant decrease of serum HDM-specific IgE and IgG1 compared to HDM-sensitized mice treated with vehicle (HDM group) (Fig. 1b). MV130 administration to HDM-sensitized mice significantly reduces HDM-induced infiltration of inflammatory cells into the airways peribronchial and perivascular areas (Fig. 1c) as well as the cell recruitment into the bronchoalveolar lavage fluid (BALF) (Fig. 1d). Remarkably, MV130 significantly reduced the number of eosinophils in BALF in HDM + MV130 group compared to sensitized mice treated with vehicle, which was also accompanied by a significant reduction in B cell, T cell, Th2 cell and ILC2 numbers without significant changes observed in the number of neutrophils (Fig. 1e, Supplementary Fig. 1). The number of macrophages was significantly reduced in the HDM group, which were restored to PBS group levels in HDM + MV130 group (Fig. 1e). These data indicate that MV130 impairs HDM allergic sensitization and HDM-induced eosinophil and inflammatory cell recruitment to the airways, which is one of the main pathological features of allergic eosinophilic asthma[26,27]. BHR, mainly driven by airway smooth muscle cell thickening and hypercontractility, is also a hallmark of asthma that significantly contributes to the main clinical symptoms during asthma attacks[27,28]. Our results show that sensitized mice receiving MV130 displayed a significantly less, or no, smooth muscle cell thickening compared to HDM-allergic mice receiving vehicle (Fig. 1f). Supporting these data, functional experiments demonstrated that MV130 treatment of sensitized mice significantly reduced enhanced pause (Penh) values after dose-dependent methacholine (Mch) challenges as an index of airway obstruction, indicating a significant reduction of bronchoconstriction in the HDM + MV130 group compared to sensitized mice receiving vehicle (HDM group) (Fig. 1g). The third key hallmark of asthma pathophysiology is goblet cell hyperplasia and mucus overproduction, which compromises the normal airway flow[27,29]. Periodic acid-Schiff (PAS)-staining experiments demonstrated that MV130 treatment of sensitized mice abolished HDM-induced mucus overproduction and restored it to basal levels (Fig. 1h). To further assess airway function, we monitored the changes in the airway resistance index (RI) after exposing mice to increasing doses of Mch. Increased Mch doses lead to significant rise in airway RI in the HDM group while airway RI values of the HDM + MV130 group resembled those of control mice for all the assayed Mch concentrations (Fig. 1i). Of note, non-significant changes in the measured parameters in Fig. 1 were observed between PBS and MV130 control non-sensitized groups indicating that mice receiving MV130 alone display a

https://doi.org/10.1038/s41467-025-62632-x

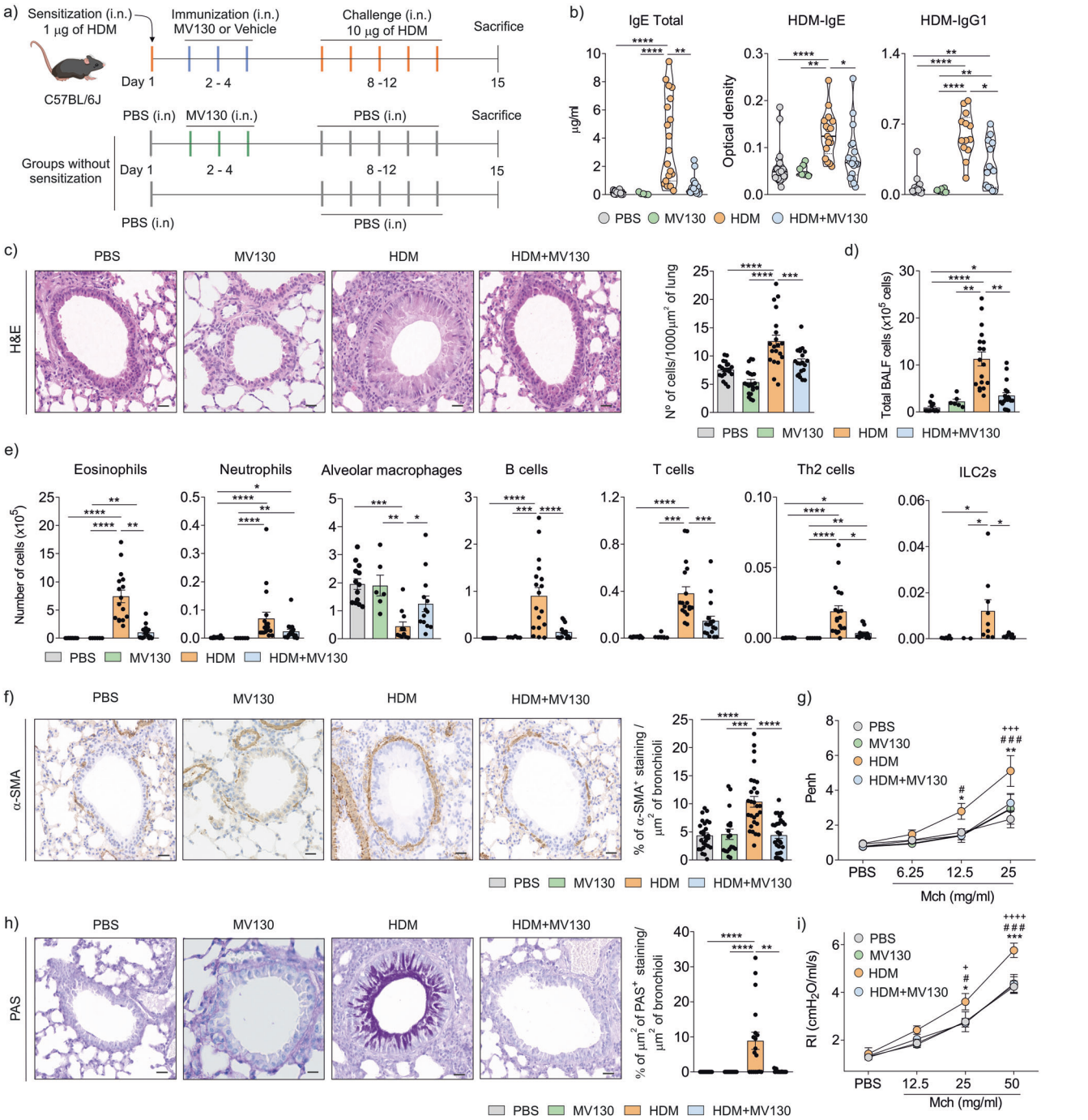


**Fig. 1 | MV130 blocks the key pathophysiological asthma features in an experimental model of HDM-induced eosinophilic allergic airway inflammation. a** Scheme of employed models. **b** Serum total IgE, HDM-specific IgE and IgG1 levels (PBS $n = 19$, MV130 $n = 5$, HDM $n = 19$, HDM + MV130 $n = 18$ mice; 4 independent experiments). **c** Left, representative hematoxylin and eosin (H&E) staining in formalin-fixed lung sections. Scale bars: 20 μm. Right, quantification of peribronchial inflammatory infiltrates in 1000 μm² of lung sections ($n = 10$ bronchioles/mouse for 2 mice per group). **d** Quantification of total cell numbers in BALF (PBS $n = 13$, MV130 $n = 6$, HDM $n = 18$, HDM + MV130 $n = 19$ mice; 4 independent experiments). **e** Quantification of different cell types in BALF (PBS $n = 13$, MV130 $n = 6$, HDM $n = 16$, HDM + MV130 $n = 17$ mice; 4 independent experiments). **f** Left, representative α-smooth muscle actin (α-SMA) staining of formalin-fixed lung sections. Scale bars: 20 μm. Right, quantification of α-SMA staining area (μm²) relative to total bronchiole area ($n = 10$ bronchioles/mouse of 2-3 mice per group). **g** Enhanced pause (Penh) measurement at increasing doses of methacholine as determined by whole-body plethysmography (WBP)[#].HDM vs MV130, *HDM vs HDM + MV130, and [+]HDM vs PBS comparisons (PBS $n = 3$, MV130 $n = 4$, HDM $n = 4$, HDM + MV130 $n = 5$ mice per experiment; a representative example of 2 independent experiments is shown). **h** Left, representative periodic acid Schiff (PAS) staining of formalin-fixed lung sections. Scale bars: 20 μm. Right, quantification of the percentage of μm² of PAS positive staining relative to μm² of bronchiole ($n = 10$ bronchioles/mouse of 2 mice per group). **i** Invasive lung function measurement of resistance index (RI) to increase doses of methacholine[#].HDM vs MV130, *HDM vs HDM + MV130, and [+]HDM vs PBS comparisons (PBS $n = 5$, MV130 $n = 4$, HDM $n = 5$, HDM + MV130 $n = 3$ mice; 3 independent experiments). Values are mean ± SEM. Statistical significance was determined using unpaired One-way ANOVA (**c** and **e** (macrophages, B and T cells)), unpaired Kruskal–Wallis (**b**, **d**, **e**, **f** and **h**), two-side unpaired Student's *t* test (**e** (ILC2s)) or unpaired Two-way ANOVA (**g** and **i**): $^{*}p < 0.05$, $^{**}p < 0.01$, $^{***}p < 0.001$ and $^{****}p < 0.0001$. Exact *p* values and source data are available in the Source Data file.

similar basal profile for the assayed parameters than those observed for the PBS control group (Fig. 1b–i). Collectively, these results demonstrate that MV130 impairs allergic sensitization and the key pathophysiological features of HDM-induced allergic eosinophilic asthma, thus restoring normal airway functionality.

### MV130 inhibits iEos recruitment without affecting homoeostatic rEos

Eosinophils have been long regarded as key pathogenic cells in the context of T2 asthma, but recent findings uncovered the existence of different lung eosinophil subsets displaying specific locations, phenotypes and functions[30,31]. Therefore, we sought to investigate in our experimental asthma model the effects of MV130 on: i) inflammatory eosinophils (iEos, Siglec-F$^{high}$ CD101$^{high}$ CD62L$^{low}$) recruited to the airways after HDM challenge and ii) homoeostatic resident eosinophils in the lung parenchyma (rEos, Siglec-F$^{int}$ CD101$^{-/low}$ CD62L$^{+}$), by quantifying their frequencies in single cell suspensions from whole lungs by flow cytometry (Fig. 2a, b, Supplementary Fig. 2). MV130 treatment significantly reduced the frequency of iEos infiltrating the airways after HDM challenge without affecting the frequency of rEos, which was similar in all the assayed conditions (Fig. 2c). To further explore the localization and frequency of the different eosinophil subsets within the tissue, we stained lung sections with specific antibodies against major basic protein (MBP) as a surrogate eosinophil marker to visualize and quantify eosinophil numbers in peribronchial areas and lung parenchyma by confocal microscopy (Fig. 2d–f). Quantification of the frequency of MBP$^{+}$ eosinophils in the whole lung sections confirmed that MV130 significantly impaired the HDM-induced eosinophil infiltration in the airways (Fig. 2d). Interestingly, this reduction was only observed within the iEos infiltrating peribronchial areas upon HDM challenge but not within rEos located in the lung parenchyma (Fig. 2e, f). These results were further confirmed by Congo Red histochemistry experiments (Fig. 2e, f). Next, we assessed the activation state of the iEos infiltrating peribronchial areas by staining lung sections with eosinophil peroxidase (EPX) and quantifying confocal microscopy images (Fig. 2g). The percentage of EPX$^{+}$ iEos was significantly reduced in peribronchial areas of mice treated with MV130 compared to vehicle-treated mice, indicating that the infiltration of activated iEos induced by HDM challenge is significantly reduced by MV130 (Fig. 2g). Supporting these data, EPX activity was also significantly decreased in BALF from mice treated with MV130 compared to vehicle-treated mice (Fig. 2h). Collectively, our data demonstrate that MV130 impairs the HDM-induced infiltration of activated iEos in the airways without affecting homoeostatic rEos.

### MV130 restores non-pathological responses to allergens in the airways

HDM-induced allergic airway eosinophilia might be driven by innate and adaptive immune responses involving ILC2s and allergen-specific Th2 cells, respectively[3,27]. Therefore, we assessed in our experimental asthma model how MV130 could impact both innate and adaptive immune responses against HDM. We first studied adaptive T cell responses by intracellular staining and flow cytometry of single cell suspensions of whole lung tissues (Supplementary Fig. 3a, b for gating strategy). MV130 significantly increased the frequency of lung IFN-γ-producing T cells compared to vehicle-treated mice, restoring the basal levels observed in the control mice (Fig. 3a). Remarkably, MV130 also significantly reduced the relative numbers of lung IL-5-producing T cells induced by HDM compared to vehicle-treated mice without significant changes in IL-10-producing T cells (Fig. 3b, c). Moreover, we observed a significant high positive correlation between the percentage of lung IL-5-producing T cells and the percentage of iEos in the airways. Additionally, there was a significant inverse correlation between the percentage of lung IFN-γ-producing T cells and the percentage of iEos (Fig. 3d). This suggests that the MV130-mediated restoration of proper T cells responses is associated with the impairment of the iEos recruitment to the airways in our HDM-induced eosinophilic allergic asthma model. Although changes in IL-10-producing T cells were not observed, MV130 treatment induced a significant increase in the frequency of lung FOXP3$^{+}$ regulatory T (Treg) cells compared to vehicle-treated and control mice (Fig. 3e). Next, we quantified the expression levels of CD23 (low affinity IgE receptor involved in IgE-mediated allergen presentation and activation of Th2 cells by DCs) on DC subsets from draining mediastinal lymph nodes (MLNs) under the different assayed conditions (Supplementary Fig. 3c for gating strategy). The percentage of CD23$^{+}$ migratory, but not resident, DCs in MLNs from vehicle-treated mice was significantly higher compared to control mice. This was restored to basal levels in MV130-treated mice, indicating that MV130 impairs the HDM-induced increase in CD23 expression on DCs migrating to MLNs (Fig. 3f).

Next, we studied the impact of MV130 treatment on the activation of ILC2s (Supplementary Fig. 3d for gating strategy). MV130 treatment significantly inhibited the HDM-induced increase of ILC2s in the lungs (Fig. 3g). Of note, a significant decrease of the percentage of HDM-induced activated IL-5-, IL-13- and IL-5/IL-13-producing ILC2s in the lung was also observed (Fig. 3g). Activated-ILC2s producing high levels of T2 cytokines significantly contribute to bronchial epithelium damage in asthma patients[3,32]. We analysed the epithelial bronchial barrier integrity in our experimental model by measuring albumin levels in BALF and quantifying lactate dehydrogenase (LDH) activity as surrogate markers of epithelial barrier leakage and damage[33,34]. MV130 treatment significantly reduced HDM-induced increased levels of albumin and LDH activity in BALF compared to vehicle-treated mice, restoring in both cases the levels observed in control mice (Fig. 3h). Supporting these data, MV130 treatment also significantly increased the mRNA expression levels of the tight junction proteins occludin and ZO-1 in the lungs compared to vehicle-treated mice (Supplementary Fig. 4). These data indicate that MV130 treatment prevents HDM-induced epithelial barrier damage in our experimental asthma model. Collectively, our results demonstrate that MV130 treatment is able to restore non-pathological local innate and adaptive immune responses in HDM-induced eosinophilic airway inflammation.

### MV130 abrogates systemic T2 immune responses in HDM-sensitised mice

To assess allergen-specific systemic responses, splenocytes of control mice (PBS or MV130 alone), vehicle-treated (HDM) and MV130-treated (HDM + MV130) groups were in vitro stimulated with HDM for 3 days (Fig. 4a). Splenocytes from vehicle-treated HDM-sensitized mice produced significantly higher levels of the T2 cytokines IL-5 and IL-13 than those from both control groups (Fig. 4b). In contrast, HDM-stimulated splenocytes from MV130-treated mice did not produce detectable levels of IL-5 and IL-13 (Fig. 4b). We did not observe significant changes in the levels of IFN-γ and IL-10 produced by HDM-stimulated splenocytes from vehicle- or MV130-treated mice (Fig. 4b). Remarkably, IL-5/IFN-γ, IL-5/IL-10, IL-13/IFN-γ, and IL-13/IL-10 ratios were significantly lower in the MV130-treated than vehicle-treated mice (Fig. 4c), indicating that MV130 treatment impairs systemic T2 immune responses without altering type 1 and IL-10 homoeostatic responses.

### MV130 prevents allergic sensitization and airway inflammation

To assess the potential capacity of MV130 to prevent allergic sensitization and eosinophilic airway inflammation in vivo, we developed a prophylactic model (Fig. 5a). Mice were i.n. administered with vehicle (HDM group) or with MV130 (MV130/HDM group) for 3 consecutive days per week for 2 weeks and then left resting 1, 2, 4 or 9 weeks prior to HDM sensitization following our conventional protocol (mice were sensitized after the resting period and challenged one week later during 5 consecutive days with HDM allergen extract) (Fig. 5a). As controls, we included a group receiving only PBS during the whole

https://doi.org/10.1038/s41467-025-62632-x

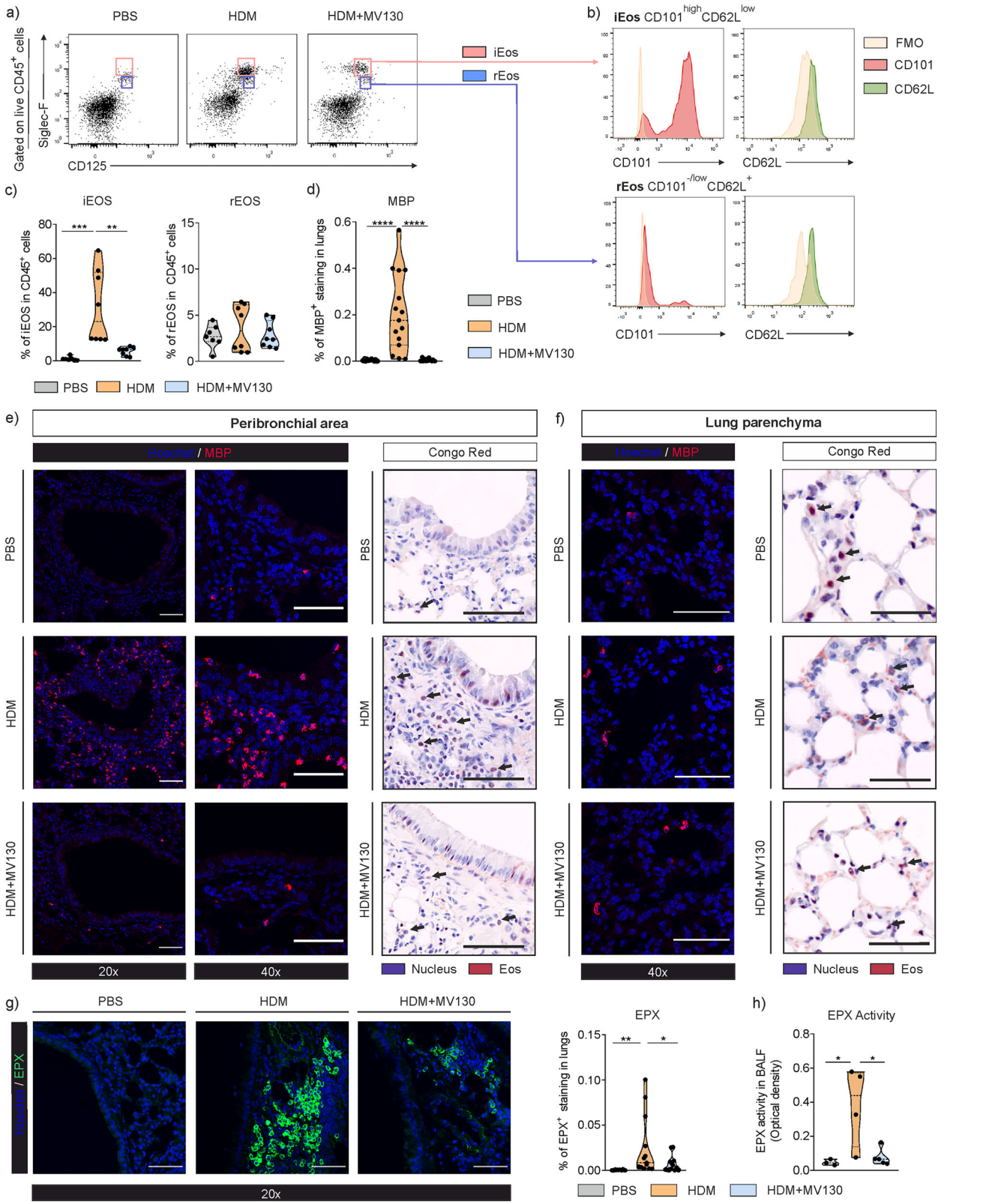


protocol (PBS group) and another group receiving prophylactic MV130 alone without subsequent HDM sensitization (MV130 group). The prophylactic treatment with MV130 prevents HDM allergic sensitization after 1, 2, 4 or 9 weeks of treatment discontinuation, as demonstrated by the significant reduction of total IgE and HDM-specific IgG1 levels compared to mice treated with vehicle (Fig. 5b). Of note, the lack of allergic sensitization in mice prophylactically treated with MV130 was also accompanied by a significant impairment of the number of inflammatory cells in BALF, including eosinophils, B cells, and Th2 cells when comparing to mice receiving vehicle for all the assayed resting periods, thus conferring long-lasting protective effects (Fig. 5c–f). Collectively, we demonstrate that the prophylactic administration of MV130 prevents allergic sensitization and eosinophilic airway inflammation in vivo in a mouse model of HDM-induced

**Fig. 2 | MV130 inhibits the HDM-induced recruitment of inflammatory eosinophils (iEos) without affecting homoeostatic resident eosinophils (rEos).** **a** Representative flow cytometry dot plots of Siglec-F and CD125 expression on live CD45$^+$ gated mouse isolated lung cells. **b** Histograms of CD101 (in red) and CD62L (in green) expression on inflammatory eosinophils (iEos) and resident eosinophils (rEos). Fluorescence minus one (FMO) of each fluorophore is shown in yellow. **c** Percentage of lung iEos and rEos relative to CD45$^+$ live lung cells ($n = 8$ mice per group; 2 independent experiments). **d** Percentage of eosinophil major basic protein (MBP) positive staining in lung sections ($n = 15$ fields/lung/mouse for 1 mouse per group). **e** Representative MBP (left) and Congo Red (right) stained mouse lung sections of the peribronchial area (1 independent experiment). Scale bars: 50 µm. Black arrows point to the eosinophils. **f** Representative MBP (left) and Congo Red (right) stained mouse lung sections of the lung parenchyma (1 independent experiment). Scale bars: 50 µm. Black arrows point to the eosinophils. **g** Left, representative eosinophil peroxidase (EPX) positive stained mouse lung sections of peribronchial area. Right, percentage of EPX positive staining in lung sections ($n = 13$ fields/lung/mouse for 1 mouse from each group). **h** Left, quantification of EPX activity in BALF (PBS $n = 3$, HDM $n = 4$, HDM + MV130 $n = 5$ mice; 1 independent experiment). Values are mean ± SEM. Statistical significance was determined using unpaired One-way ANOVA (**c**, **g** and **h**) and unpaired Kruskal–Wallis test (**d**): $^*p < 0.05$, $^{**}p < 0.01$, $^{***}p < 0.001$ and $^{****}p < 0.0001$. Exact $p$ values and source data are available in the Source Data file.

eosinophilic airway inflammation up to 9 weeks of treatment discontinuation.

## MV130 impairs HDM-induced T2 allergic profile by regulating human DCs

To assess the capacity of MV130 to interfere with the development of HDM-induced T2 immune responses in humans, we first stimulated human peripheral blood mononuclear cells (PBMCs) from healthy donors with vehicle (Ctrl-), MV130 alone, HDM alone or in combination with MV130 for 4 days. MV130-stimulated PBMCs produced significantly higher levels of IFN-γ and IL-10, and lower levels of IL-5 compared to unstimulated PBMCs (Supplementary Fig. 5a). HDM + MV130-stimulated PBMCs produced significantly lower levels of IL-5 and significantly higher levels of IFN-γ and IL-10 than HDM-stimulated PBMCs in culture supernatants after 4 days of stimulation (Suplemmentary Fig. 5a). Consequently, the IFN-γ/IL-5 and IL-10/IL-5 ratios were significantly higher in HDM + MV130-stimulated PBMCs than PBMCs stimulated with HDM alone, indicating that MV130 is able to shift the cytokine signature imprinted by HDM in PBMCs from a Th2 allergic profile to a Th1 and IL-10 non-pathogenic immune responses to allergens (Suplemmentary Fig. 5b). Considering the key role of DCs in the orchestration of T cell responses and allergic sensitization, we wanted to further explore how MV130 directly immunomodulates human DCs' responses in the presence of HDM. For that purpose, we purified monocytes from PBMCs of healthy and HDM-allergic asthmatic donors and generated human monocyte-derived DCs (HmoDCs) following conventional protocols (Fig. 6a)[35]. Stimulation of HmoDCs from healthy and allergic asthma patients with MV130 alone significantly increased the production of TNF-α, IL-6 and IL-10 compared to vehicle-stimulated HmoDCs (Fig. 6b). Similarly, HDM + MV130-stimulated HmoDCs from both healthy and asthma patients produced significantly higher levels of pro-inflammatory TNF-α, IL-6 and the anti-inflammatory IL-10 cytokines than HDM-stimulated HmoDCs, suggesting that MV130 promotes type 1/IL-10 anti-allergic profiles in both healthy and allergic asthma patients HmoDCs (Fig. 6b). To further confirm these findings, we co-cultured HmoDCs from healthy or allergic asthma donors with allogeneic naïve CD4$^+$ T cells in the presence of the different stimuli as previously (Fig. 6c)[35]. Of note, this in vitro experimental allogenic setting allowed us to explore how MV130 regulates the polarization capacity of HmoDCs in the presence of HDM in a non-antigen specific manner upon T cell activation due to mismatch of MHC molecules. MV130-stimulated HmoDCs from healthy and asthmatic donors generated T cells producing higher levels of IFN-γ and IL-10 than those generated by vehicle-stimulated HmoDCs without detection of IL-5 production (Fig. 6d, e). T cells generated by HDM + MV130-stimulated HmoDCs from both healthy and allergic asthma patients produced significantly higher IFN-γ and IL-10 than those generated by HmoDCs stimulated with HDM alone. In addition, T cells generated by HDM + MV130-stimulated HmoDCs from healthy donors showed a significant reduction of IL-5 production than those generated by HDM-stimulated HmoDCs, which was not observed for allergic asthma patients (Fig. 6d, e). Of note, the IFN-γ/IL-5 and IL-10/IL-5 ratios were significantly higher in the co-cultures of T cells and HmoDCs from both healthy and asthmatic patients upon stimulation with HDM + MV130 compared to stimulation with HDM alone (Fig. 6d, e). Collectively, all these data demonstrate that MV130 counteracts the Th2 polarization capacity imprinted by HDM to HmoDCs from healthy and allergic asthmatic patients by endorsing a shift towards Th1 and IL-10, which might well promote non-pathological immune responses to the allergens contained in HDM.

## MV130 induces transcriptomic and metabolic rewiring in human DCs

To gain insight into the molecular mechanisms involved in the mode of action of MV130 on human DCs underlying the capacity to prevent allergic sensitization, we performed gene set enrichment analysis (GSEA) using our previous global comparative transcriptomic analysis microarray dataset (deposited in E-MTAB-5259) from MV130- vs vehicle-stimulated HmoDCs from healthy donors[20,36]. MV130-stimulated HmoDCs displayed a significant enrichment of the pro-inflammatory TNF-α-, IFN-γ-, IL-6-, and the anti-inflammatory IL-10-mediated signalling pathways (Fig. 7a), which is fully in agreement with our experimental results (Fig. 6b, d). TNFAIP3 (A20), IRF7 or CD274 (PDL1) genes, previously reported to be downregulated in asthmatic patients and whose expression levels correlates with the "farm protective effect"[37], were highly enriched in MV130-stimulated HmoDCs (Fig. 7b). Compared to MV130-stimulated HmoDCs, vehicle-stimulated HmoDCs showed a significant enrichment in the asthma pathway gene set (Fig. 7a) and in the high-affinity receptor for IgE (FcεRI)-signalling pathway, which play a key role in allergic asthma (Fig. 7b). These data strongly support that MV130 displays anti-allergic eosinophilic asthma features by imprinting human DCs with the capacity to generate type 1 immune responses with IL-10 production. In addition to immune signalling pathways, GSEA showed important metabolic gene sets differently enriched between groups. mTOR signalling pathway, a key regulator of energetic metabolism, and glycolysis pathway gene sets were significantly enriched in MV130-stimulated HmoDCs (Fig. 7a, c). To validate these data, we determined the real-time glycolytic proton efflux rate (glycoPER) of vehicle (Ctrl-)- or MV130-stimulated HmoDCs using a Seahorse analyser. MV130-stimulated HmoDCs showed an enhanced glycolytic metabolism in basal conditions (basal glycolysis) and after inhibition of the electron transport chain (compensatory glycolysis) compared to control-stimulated HmoDCs (Supplementary Fig. 6). Next, we wanted to investigate whether MV130-induced enhanced glycolysis could be also sustained in HDM-stimulated HmoDCs. For that, HmoDCs were stimulated with vehicle (Ctrl-), HDM or HDM + MV130 for 24 h and the metabolic dynamic changes were monitored in a Seahorse analyser (Fig. 7d). HDM/MV130-stimulated HmoDCs showed a significantly higher basal glycolysis and compensatory glycolysis than HmoDCs stimulated with HDM alone (Fig. 7e). GSEA also showed that OXPHOS and tricarboxylic acid (TCA) signalling pathways were significantly enriched in vehicle-stimulated HmoDCs (Fig. 7a, f). HDM + MV130-stimulated HmoDCs showed a significant reduction of the mitochondrial membrane potential without significant changes in the mitochondrial mass compared to

https://doi.org/10.1038/s41467-025-62632-x

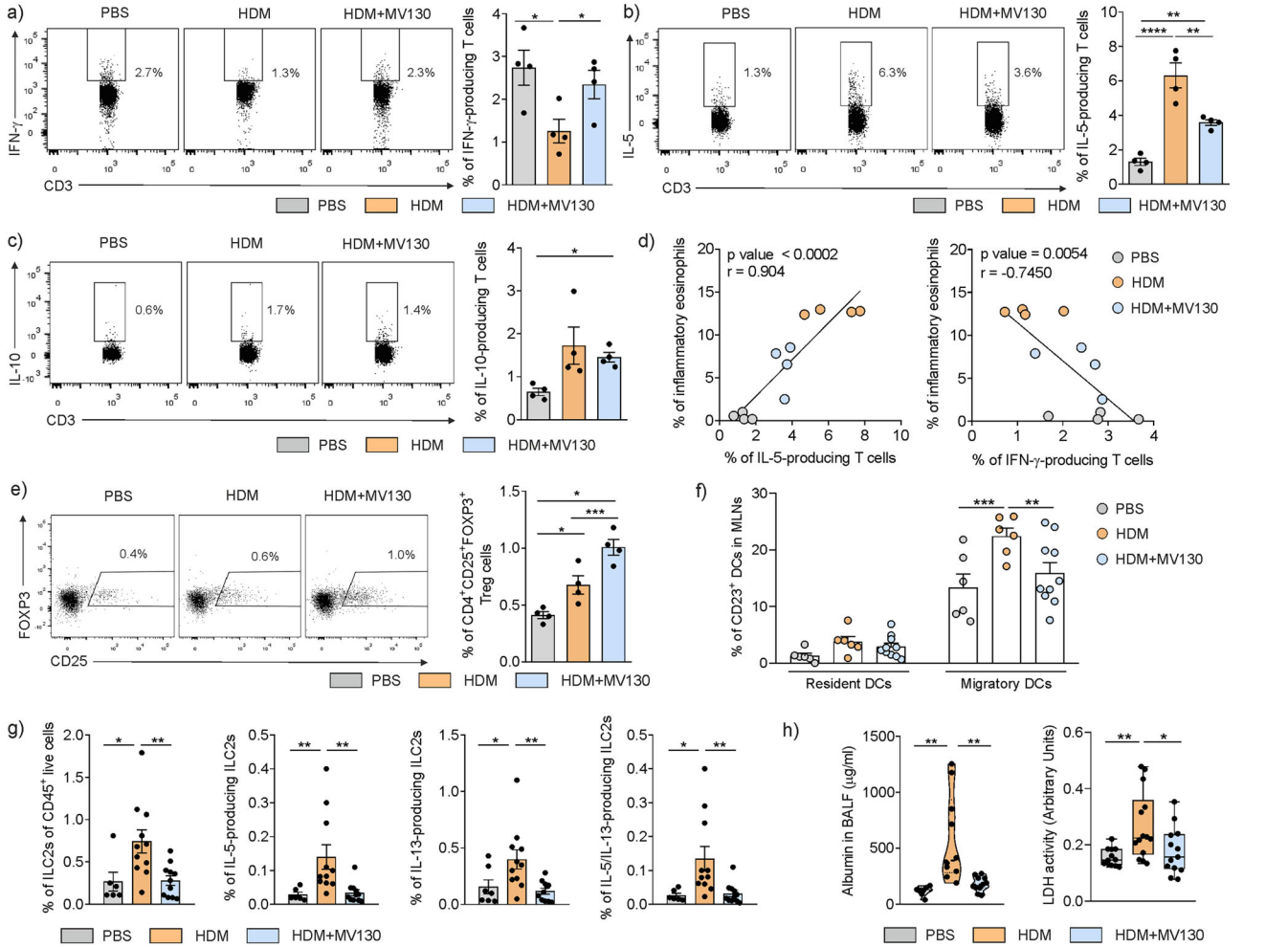


**Fig. 3 | MV130 restores non-pathological innate and adaptive immune responses against HDM.** Left, representative flow cytometry dot plots of intracellular staining of IFN-γ- (**a**), IL-5- (**b**) or IL-10-producing (**c**) lung T cells, respectively, relative to $CD3^+$ lung T cells. Right, percentage of IFN-γ-, IL-5- or IL-10-producing lung T cells, respectively, relative to $CD3^+$ lung T cells ($n = 4$ mice per group of one representative experiment out of 2). **d** Correlation between the percentage of iEos and the % of IL-5− (left) and IFN-γ- (right) producing lung T cells, respectively. "r" indicates Pearson correlation coefficient. **e** Left, representative flow cytometry dot plots of $CD4^+CD25^+FOXP3^+$ lung Treg cells. Right, percentage of $CD4^+CD25^+FOXP3^+$ Treg cells relative to live cells in the lungs ($n = 4$ mice per group of one representative experiment out of 2). **f** Percentage of $CD23^+$ resident and migratory DCs in mediastinal lymph nodes (MLNs) (PBS $n = 6$, HDM $n = 6$, HDM + MV130 $n = 10$ mice; 2 independent experiments). **g** Percentage of total ILC2s, and IL-5-, IL-13- and IL-13/IL-5-producing ILC2s of $CD45^+$ live lung cells (PBS $n = 6$, HDM $n = 11$, HDM + MV130 $n = 11$ mice; 2 independent experiments). **h** Left, levels of serum albumin in BALF 24 h after last HDM challenge (PBS $n = 7$, HDM $n = 10$, HDM + MV130 $n = 11$ mice; 2 independent experiments). Right, lactate dehydrogenase (LDH) levels in BALF 72 h after last HDM challenge (PBS $n = 12$, HDM $n = 14$, HDM + MV130 $n = 13$ mice; 2 independent experiments). Values are mean ± SEM. Statistical significance was determined using two-side unpaired Student's $t$ test (**a**), unpaired One-way ANOVA (**b**, **e**, and **h**), unpaired Kruskal–Wallis test (**c** and **g**), two-side Pearson test (**d**) and unpaired Two-way-ANOVA (**f**): $^*p < 0.05$, $^{**}p < 0.01$, $^{***}p < 0.001$ and $^{****}p < 0.0001$. Exact $p$ values and source data are available in the Source Data file.

HmoDCs stimulated with HDM alone, resulting in a significantly lower mitochondrial membrane potential/mitochondrial mass ratio in HDM + MV130-stimulated HmoDCs (Fig. 7g). Collectively, MV130 induces transcriptional and metabolic programmes in human DCs characterized by the activation of TNF-α-, IFN-γ-, IL-6-, and IL-10-mediated pathways as well as by increased glycolysis and reduced OXPHOS, which might well contribute to the restoration of non-pathological immune responses against HDM-induced airway eosinophilic inflammation.

### Adoptive transfer of MV130-BMDCs prevents airway inflammation via MyD88

To assess the potential direct contribution of DCs to the MV130 anti-allergic effects in vivo, bone marrow-derived DCs (BMDCs) from wild type C57BL/6J mice were generated, stimulated for 18 h with vehicle (Vehicle-BMDCs) or MV130 (MV130-BMDCs) and i.n. transferred to wild type mice on day one. After 8 h of BMDCs adoptive transfer, mice were sensitized and challenged with HDM following our conventional protocol (Vehicle-BMDCs/HDM and MV130-BMDCs/HDM groups) (Fig. 8a). As control, we included a group receiving only PBS during the whole protocol (PBS group). Intranasal administration of MV130-BMDCs prevented HDM allergic sensitization as demonstrated by the significant reduction of total IgE, HDM-specific IgG1 and IgE levels compared to mice treated with Vehicle-BMDCs (Fig. 8b). Of note, mice transferred with MV130-BMDCs displayed a significant impairment of the total number of cells in BALF, including eosinophils, neutrophils, B cells, T cells and Th2 cells compared to the Vehicle-BMDCs/HDM group (Fig. 8c, d). Collectively, our airway adoptive transfer experiments demonstrate that MV130-BMDCs prevent allergic sensitization and eosinophilic airway inflammation in vivo, reinforcing the important role played by DCs in the MV130 protective effects. We have previously shown that TLR- and NOD-mediated signalling pathways contribute to immune responses in MV130-activated human DCs[20]. To gain deeper insights into the molecular mechanisms involved in the MV130-imprinted effects in DCs and in the observed in vivo anti-

https://doi.org/10.1038/s41467-025-62632-x

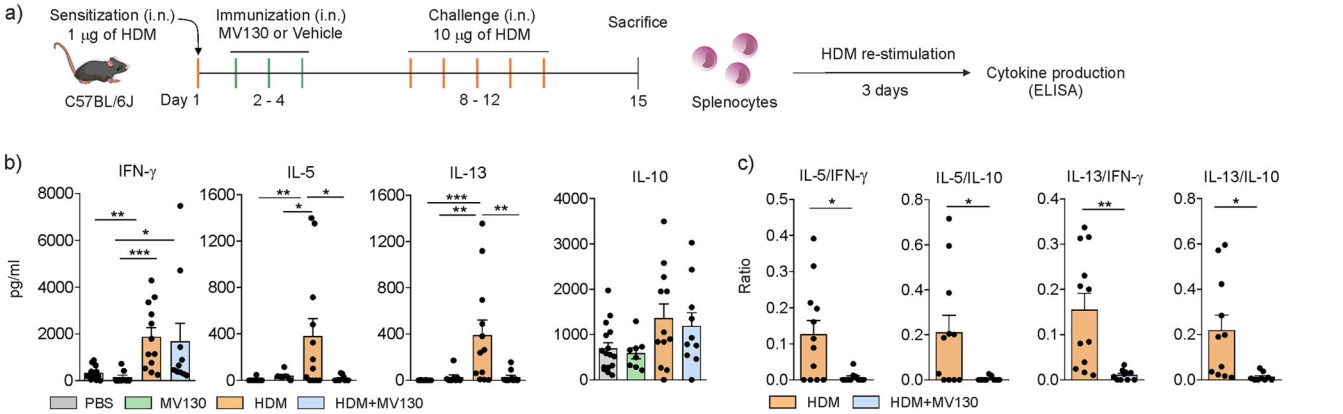


**Fig. 4 | MV130 abrogates systemic T2 immune responses in HDM-sensitised mice. a** Schematic representation of the model employed to assess in vitro responses of splenocytes from the different groups after HDM stimulation. **b** Cytokine production after 3 days of stimulation of splenocytes with HDM from the different groups (PBS $n = 15$, MV130 $n = 8$, HDM $n = 12$, HDM + MV130 $n = 10$ mice; 4 independent experiments). **c** Ratios of cytokine production (HDM $n = 12$, HDM + MV130 $n = 10$ mice; 4 independent experiments). Values are mean ± SEM. Statistical significance was determined using unpaired One-way ANOVA (**b**), unpaired Kruskal–Wallis (**b**, IFN-ɣ) and two-side unpaired Student's $t$ test (**c**): $^{*}p < 0.05$, $^{**}p < 0.01$ and $^{***}p < 0.001$. Exact $p$ values and source data are available in the Source Data file.

allergic capacity, BMDCs were in vitro generated from wild type and MyD88$^{-/-}$ C57BL/6J mice (Fig. 8e). Both BMDCs types were stimulated with vehicle (Ctrl-), MV130, or with MV130 after previous incubation with Gefitinib (a pharmacological inhibitor of RIPK2, the adaptor protein of NOD1/NOD2-mediated signalling pathways) (Fig. 8e). MV130 stimulation significantly increased the expression of CD40 (a key molecule previously involved in the tolerogenic effects of IL-10 regulatory DCs)[38] in wild type and MyD88$^{-/-}$ BMDCs compared to control and Gefitinib/MV130 groups (Fig. 8f). MV130-induced CD40 expression was significantly higher in wild type than MyD88$^{-/-}$ BMDCs, indicating the important contribution of MyD88-mediated signalling pathways coupled to TLRs in such induction (Fig. 8f). Gefitinib significantly reduced the MV130-induced expression of CD40 in wild type and MyD88$^{-/-}$ BMDCs, reaching only basal levels in MyD88$^{-/-}$ BMDCs, indicating that NOD-mediated signalling pathways partially contribute to MV130-induced CD40 expression in BMDCs (Fig. 8f). Of note, MV130-induced cytokine production (TNF-α, IL-6 and IL-10) was abolished in MyD88$^{-/-}$ BMDCs compared to wild type BMDCs in all the assayed conditions, indicating TLRs-mediated signalling as the main pathways involved in the cytokine signature imprinted by MV130 in BMDCs (Fig. 8g). Gefitinib significantly reduced the production of all the assayed cytokines in MV130-stimulated wild type BMDCs without reaching basal levels in any case, indicating that NOD-mediated pathways might also partially contribute to MV130-induced cytokine production but at a lesser extent than TLRs (Fig. 8g). Therefore, we assessed the impact of MyD88 inhibition in the in vivo anti-allergic effects of MV130-BMDCs using the airway adoptive transfer model previously described (Fig. 8a). MyD88$^{-/-}$ BMDCs were stimulated with vehicle (Vehicle-MyD88$^{-/-}$ BMDCs) or MV130 (MV130-MyD88$^{-/-}$ BMDCs) for 18 h and then i.n. administered to mice. After 8 h of MyD88$^{-/-}$ BMDCs adoptive transfer, mice were sensitized and challenged with HDM following our conventional protocol (Fig. 8a). Of note, MV130-stimulated MyD88$^{-/-}$ BMDCs were not able to prevent HDM allergic sensitization showing no significant differences in total IgE or HDM-specific IgG1 levels compared to mice treated with vehicle-stimulated MyD88$^{-/-}$ BMDCs (Fig. 8h). Similarly, mice treated with MV130-MyD88$^{-/-}$ BMDCs displayed similar numbers of total cells in BALF, eosinophils, neutrophils, B cells, T cells and Th2 cells than mice treated with vehicle-MyD88$^{-/-}$ BMDCs (Fig. 8I, j). These data indicate that MV130-stimulated BMDCs from MyD88$^{-/-}$ mice did not prevent HDM allergic sensitization and eosinophilic airway inflammation in vivo, demonstrating that MyD88-mediated signalling pathways coupled to activated TLRs are crucial for the asthma preventive effect of MV130-treated BMDCs.

## Discussion

In this study, we uncover the unpreceded property of the mucosal vaccine MV130 to prevent HDM allergic sensitization as well as HDM-induced local and systemic T2 immune responses and associated eosinophilic airway inflammation. MV130 abolished all the key pathophysiological and clinical features associated with asthma in an in vivo experimental mouse model of HDM-induced allergic eosinophilic asthma. We demonstrated that MV130 promotes non-pathological innate and adaptive immune responses against HDM by inhibiting HDM-induced Th2 cells and ILC2s in vivo, which impairs the recruitment of iEos into the bronchial mucosa without affecting homoeostatic rEos in the lung parenchyma, thus restoring normal airway functionality. MV130 also impairs allergen-specific IgE sensitization and systemic T2 immune responses without altering type 1 and IL-10 homoeostatic responses. Of note, our data demonstrated that the prophylactic administration of MV130 prevents allergic sensitization and HDM-induced eosinophilic airway inflammation in vivo up to 9 weeks after treatment discontinuation, thus demonstrating long-lasting protective effects. In addition, we showed in human DCs from both healthy and HDM-allergic asthma donors that MV130 counteracts the Th2 polarization capacity imprinted by HDM and endorses a shift towards Th1 and IL-10 immune responses. Mechanistically, MV130 induces transcriptional programs in human DCs leading to the activation of TNF-α-, IFN-γ-, IL-6- and IL-10-mediated pathways and imprints metabolic reprogramming with increased glycolysis and reduced OXPHOS, which might well contribute to the generation of non-pathological immune responses to the allergens. In vivo airway transfer experiments demonstrated that MV130-treated BMDCs suppress HDM-induced eosinophilic airway inflammation through mechanisms partially dependent on MyD88-mediated signalling pathways, thus reinforcing the key role played by DCs in these effects. Our findings might well contribute to open future interventions based on mucosal whole heat-inactivated PBPs to prevent allergic airway inflammation and to reduce the risk of allergic asthma development.

Asthma represents a major health problem affecting around 400 million people in the world, being T2 allergic eosinophilic asthma the most common pheno-endotype[2,39]. Corticosteroids and bronchodilators remain the mainstay asthma treatment, but the prevention and management of severe asthma continues to be challenging[1,3].

https://doi.org/10.1038/s41467-025-62632-x

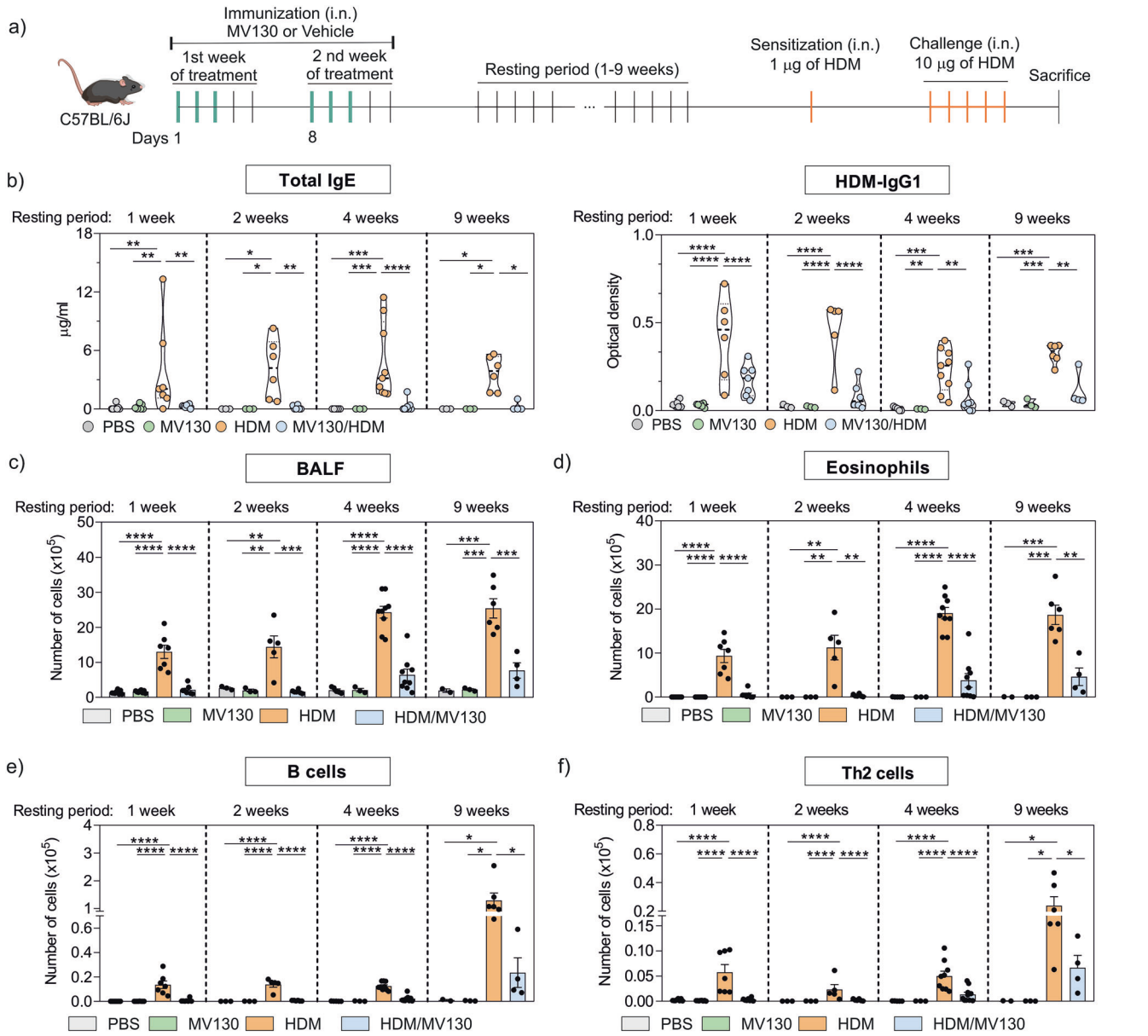


**Fig. 5 | MV130 prophylactic treatment prevents allergic sensitization and HDM-induced eosinophilic airway inflammation, conferring protection up to 9 weeks after treatment discontinuation. a** Schematic representation of the prophylactic treatment with MV130 or vehicle, resting period (1, 2, 4 or 9 weeks) and following HDM-induced asthma model. Two control groups without sensitization were included, MV130 group receiving PBS in the sensitization and challenge and MV130 during immunization and a PBS group receiving only PBS; i.n., intranasal. **b** Serum total IgE, HDM-specific IgG1 levels ($n = 3–9$ mice from each group; 2 independent experiments). **c** Quantification of total cell numbers of different populations in bronchoalveolar lavage fluid (BALF) as determined by flow cytometry ($n = 3–9$ mice from each group; 2 independent experiments). **d** Quantification of total cell numbers of eosinophils, **e** B cells and **f** Th2 cells in BALF ($n = 3–9$ mice from each group; 2 independent experiments). Values are mean ± SEM. Statistical significance was determined using unpaired Two-way ANOVA (**b**) and unpaired One-way ANOVA (**c**–**f**) tests: $^{*}p < 0.05$, $^{**}p < 0.01$, $^{***}p < 0.001$ and $^{****}p < 0.0001$. Exact $p$ values and source data are available in the Source Data file.

Biologicals have demonstrated efficacy in reducing exacerbations, improving lung function, and reducing oral corticosteroid use, but their main drawbacks include the high costs, the lack of suitable biomarkers and not yet firmly demonstrated disease-modification capacity[1–3,39]. Allergen-specific immunotherapy consisting in the administration of high doses of the causative allergens to induce tolerance is able to modify the course of the disease, but it is not recommended for severe asthma due to safety concerns[1,2,39]. Therefore, there is an unmet need for the development of strategies for asthma prevention and treatment.

A plethora of epidemiologic, preclinical, and clinical studies uncovered the protective role of living in a farming environment ("farm protective effect") and specific microbial exposure early in life for the prevention of asthma and other allergic diseases[40–42]. These data focused the actual research on mimicking, with standardized products, the beneficial properties of that environmental exposure[11,16,17,37,43]. In this context, different types of PBPs, specific bacterial species or microbial-derived products are in the spotlight due to the demonstrated capacity to prevent recurrent viral infections, which is together with allergic sensitization a main risk factor for asthma development[13–17]. Among these PBP, the mucosal MV130 vaccine has demonstrated preclinical and clinical efficacy against viral infections through mechanisms dependent on TI, being the first PBP described with these properties[14,15,21,44]. Therefore, it is reasonable to

https://doi.org/10.1038/s41467-025-62632-x

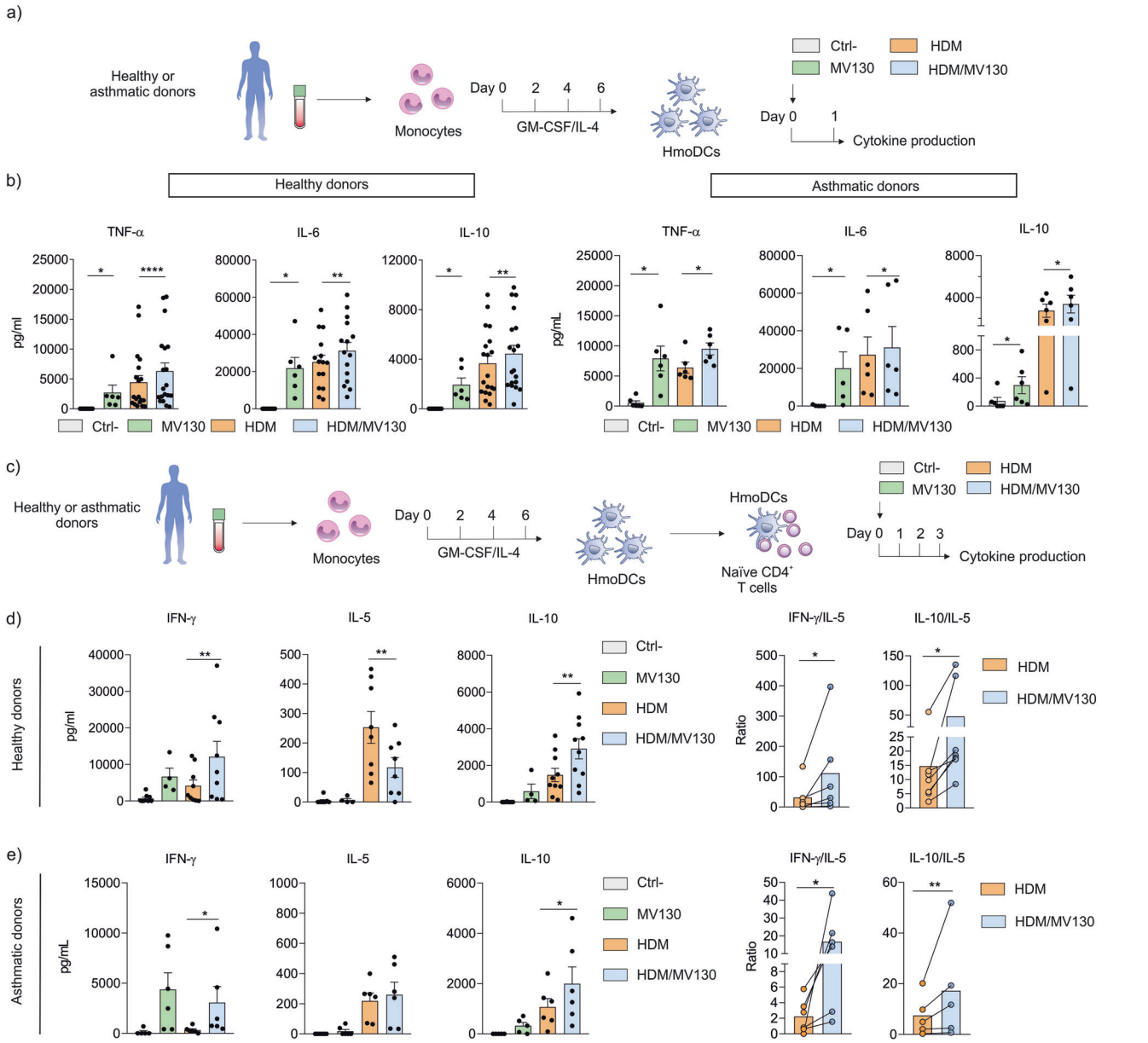


**Fig. 6 | MV130 impairs HDM-induced T2 allergic profile by generating human DCs with the capacity to polarize Th1 and IL-10 immune responses. a** Scheme of the employed protocol for HmoDCs generation from healthy and HDM-allergic asthmatic donors and in vitro stimulation. **b** Cytokine production in cell-free supernatants after stimulation of HmoDCs with vehicle (Ctrl-), MV130, HDM or HDM/MV130 for 24 h (Ctrl- $n = 17$, MV130 $n = 6$, HDM $n = 19$, HDM + MV130 $n = 19$ healthy donors and Ctrl- $n = 6$, MV130 $n = 6$, HDM $n = 6$, HDM + MV130 $n = 6$ asthmatic donors). **c** Scheme of the employed protocol for HmoDCs and allogeneic naïve T cells co-cultures. **d** Left, cytokines produced by allogeneic naïve $CD4^+$ T cells primed by HmoDCs in the presence of vehicle (Ctrl-), MV130, HDM or HDM/MV130 after 3 days (Ctrl- $n = 9$, MV130 $n = 4$, HDM $n = 9$, HDM + MV130 $n = 9$ healthy donors). Right, ratios of indicated cytokines were determined for HDM and HDM/MV130 stimulations (HDM $n = 7$, HDM + MV130 $n = 7$ healthy donors). **e** Left, cytokines produced by allogeneic naïve $CD4^+$ T cells primed by HmoDCs in the presence of vehicle (Ctrl-), MV130, HDM or HDM/MV130 ($n = 6$ asthmatic donors). Right, ratios of indicated cytokines were determined for HDM and HDM/MV130 stimulations ($n = 6$ asthmatic donors). Values are mean ± SEM. Statistical significance was determined using two-side paired Wilcoxon or Student's $t$ test (**b**, **d**, **e**) depending on the normal distribution of the compared samples analysed by D'Agostino-Pearson normality test: $^*p < 0.05$, $^{**}p < 0.01$ and $^{****}p < 0.0001$. Exact $p$ values and source data are available in the Source Data file.

foresee that avoiding early viral infection with MV130 could prevent the development of wheezing attacks and asthma exacerbation in children[22]. Nonetheless, the potential capacity of MV130 to impair T2 eosinophilic allergic airway inflammation remained unknown. Different non-specific strategies for HDM-induced airway inflammation have been previously assayed with diverse outcomes, including TLR7 agonists, CpG motifs encapsulated in viral-like particles, non-specific mRNA lipid nanoparticles, living or heat-inactivated lactic acid bacteria strains among others, suggesting bacteria and bacteria-derived products as potential suitable strategies for the prevention and treatment of allergic asthma[45–48].

Here, we show that MV130 prevents eosinophilic airway inflammation in an in vivo experimental mouse model of HDM-induced allergic eosinophilic asthma by restoring local and systemic innate and adaptive immune responses. Other PBPs such as OM-85 or specific interventions with *Acinetobacter lwoffii* have the capacity to prevent eosinophilic airway inflammation at the local level when administered via the i.n. route[18,19]. We also demonstrate that MV130 not only impairs

https://doi.org/10.1038/s41467-025-62632-x

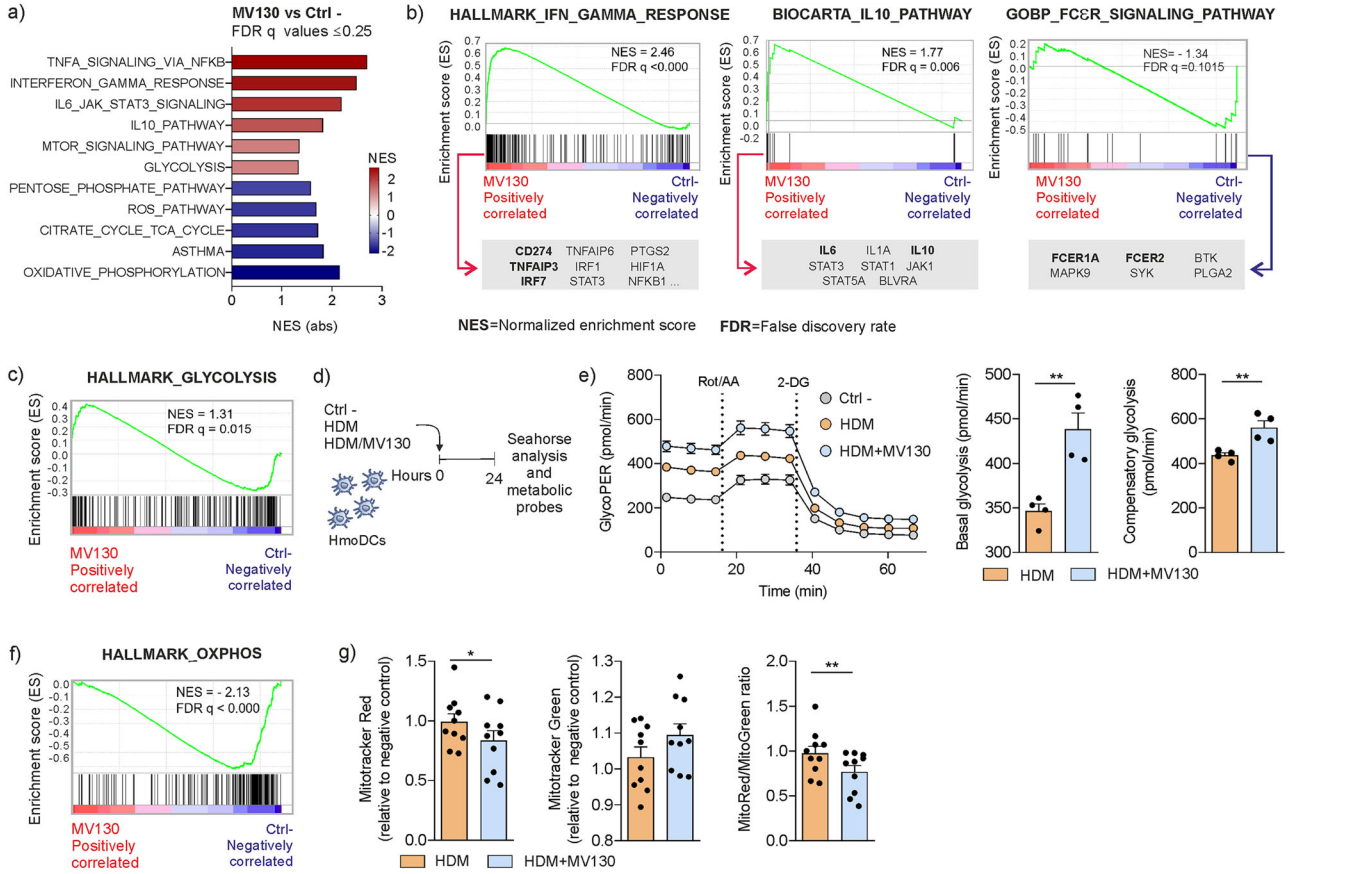


**Fig. 7 | MV130 imprints transcriptomic and metabolic rewiring in human DCs.** **a** Bar plot showing gene set enrichment analysis (GSEA) the selected significantly enriched gene sets for HALLMARK, KEGG, GOBP and BIOCARTA data bases from 24 h MV130- vs vehicle (Ctrl-)-stimulated HmoDCs Gene Array ($n = 4$ healthy donors). Enriched gene sets in MV130-stimulated HmoDCs were represented in red and vehicle (Ctrl-)-stimulated HmoDCs were represented in blue. NES (Abs), NES absolute value. All FDR $q$ values < 0.25. **b** GSEA for HALLMARK_IFN-GAMMA_RESPONSE, BIOCARTA_IL-10_PATHWAY and GOBP_FCεR_SIGNALING_PATHWAY gene sets showing the genes enriched in the indicated biological pathways differentially enriched in MV130- or vehicle (Ctrl-)-stimulated HmoDCs ($n = 4$ healthy donors). **c** GSEA for HALLMARK_GLYCOLISIS gene set significantly enriched in MV130-stimulated HmoDCs from Gene Array results ($n = 4$ healthy donors). **d** Scheme of the employed protocol with HmoDCs for in vitro metabolic studies. **e** Left, real-time analysis of glycolytic Proton Efflux Rate (glycoPER) of HmoDCs after stimulation with HDM, HDM + MV130 or vehicle (Ctrl-) by sequential addition of rotenone/antimycin A (Rot/AA), and 2-deoxyglucose (2-DG). Right, quantification of basal and compensatory glycolysis ($n = 4$ healthy donors). **f** GSEA for HALLMARK_OXPHOS gene set significantly enriched in vehicle (Ctrl)-treated HmoDCs from Gene Array results ($n = 4$ healthy donors). **g** Fluorescence intensity of HDM- or HDM + MV130-stimulated HmoDCs stained with MitoTracker™ Red CMXRos (mitochondrial membrane potential) and MitoTracker™ Green FM (mitochondrial mass) relative to negative control-stimulated cells. MitoTracker Red/MitoTracker Green ratio is also shown ($n = 10$ healthy donors). Values are mean ± SEM. Statistical significance was determined using two-side paired Student's $t$ test (**e** and **g**): $^{*}p < 0.05$, and $^{**}p < 0.01$. Exact $p$ values and source data are available in the Source Data file.

airway eosinophilia but also abolishes HDM-specific IgE sensitization and systemic allergen-specific T2 responses. MV130 treatment significantly reduced the percentage of CD23$^{+}$ migratory DCs in MLNs. CD23 expression on antigen presenting cells plays a key role in the activation of allergen-specific Th2 cells during recall responses via facilitated antigen presentation[49,50]. In addition, our GSEA showed that FcεRI-signalling pathway is enriched in human DCs at the steady state compared to MV130-stimulated human DCs. We have previously shown that blocking allergen-induced IgE-FcεRI crosslinking with monoclonal antibodies targeting IgE impairs the capacity of human plasmacytoid DCs to generate Treg cells[51,52]. All these data indicate that MV130 downregulates the expression of both high- and low-affinity receptors for IgE on DCs as a mechanism by which this mucosal vaccine might well promote non-pathological adaptive immune responses against allergens.

In addition to blocking systemic IgE sensitization, MV130 abolished all the clinical features associated with asthma, including airway eosinophilia, BHR, mucus production and epithelial barrier damage, which resulted in the restauration of normal airway functionality. At the local airways, MV130 increased IFN-γ-producing Th1 cells, IL-10-producing T cells and FOXP3$^{+}$ Treg cells whereas inhibited both IL-5-producing Th2 cells and IL-5/IL-13-producing ILC2s, which impaired iEos infiltration into the bronchial mucosa without affecting homoeostatic rEos. Of note, instead of the detrimental role of iEos in asthma, rEos in the lung parenchyma display homoeostatic functions and have been found to inhibit the maturation and pro-Th2 function of allergen loaded DCs[30,31]. Epithelial barrier dysfunction is a major driver of asthma development as compromise the defence against viral infections and enhances the risk of allergic sensitization and asthma attacks[53–55]. Smooth muscle layer thickening and Goblet cell hyperplasia also contributes to worsening BHR, airway remodelling and lung function decline[26,27]. In our experimental asthma model, MV130 also significantly impaired HDM-induced epithelial barrier damage, smooth muscle thickening and mucus overproduction, which together with the inhibition of airway eosinophilia contribute to reduce BHR and to restore normal airway functionality. Despite these promising in vivo results, one major limitation of our study is that we only used one mouse strain (C57BL/6J) and allergen model (HDM) to assess the anti-allergic effects of MV130 as a proof-of concept. Future studies using

https://doi.org/10.1038/s41467-025-62632-x

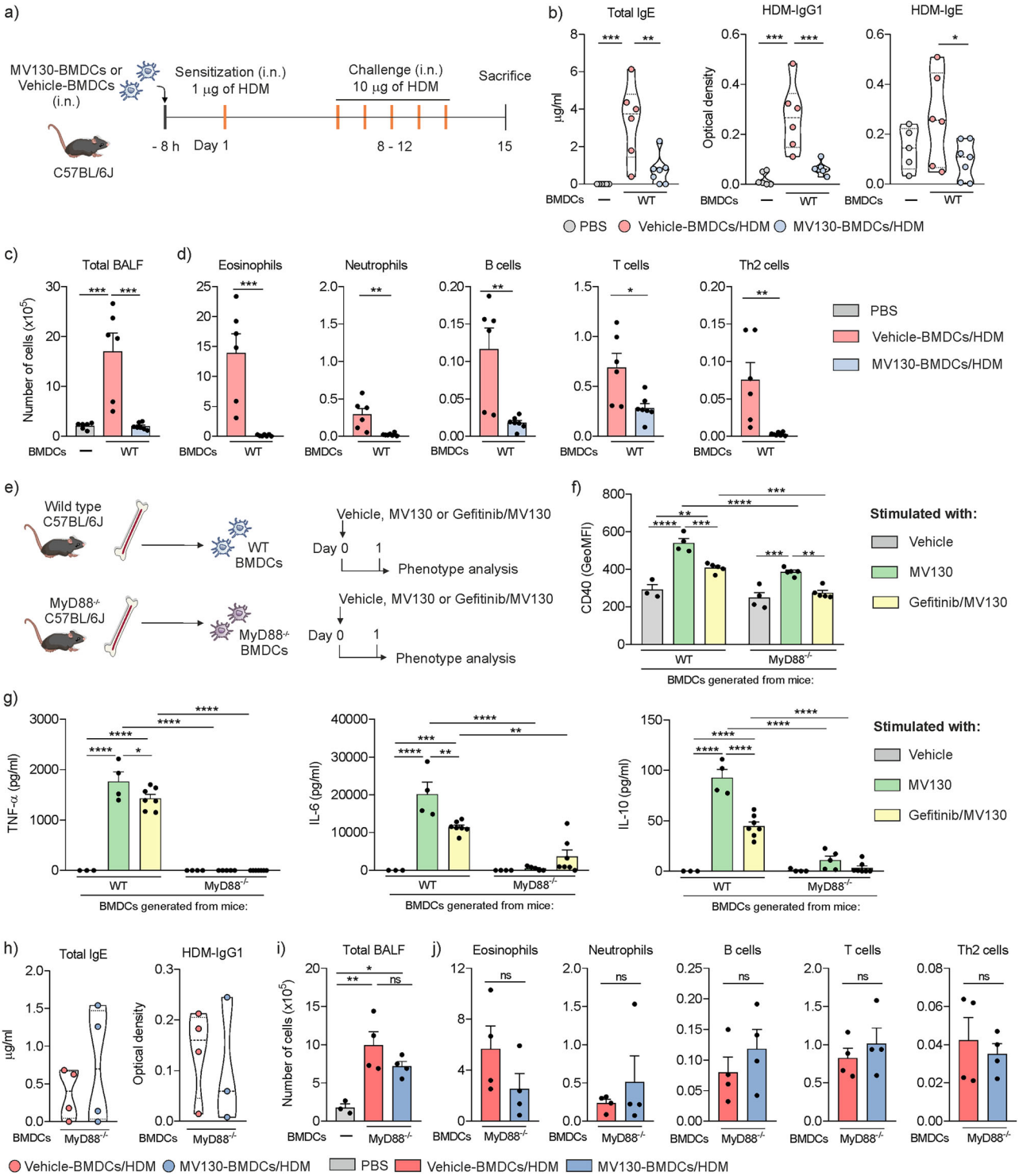


**Fig. 8 | MV130 reprograming of BMDCs via MyD88-mediated pathways prevents HDM-induced eosinophilic allergic airway inflammation. a** Schematic representation of MV130-BMDCs or vehicle-BMDCs intranasal administration and following HDM-induced asthma model. **b** Serum total IgE and HDM specific IgE and IgG1 levels (PBS $n = 6$, Vehicle-BMDCs/HDM $n = 6$, MV130-BMDCs/HDM $n = 7$ mice; 2 independent experiments). **c** Quantification of total cell numbers and **d** of different cell types in BALF determined by flow cytometry (PBS $n = 6$, Vehicle-BMDCs/HDM $n = 6$, MV130-BMDCs/HDM $n = 7$ mice; 2 independent experiments). **e** Schematic representation of bone marrow progenitors from wild type and MyD88$^{-/-}$ mice differentiation to BMDCs and following in vitro stimulation with vehicle (Ctrl-), MV130, or Gefinitib/MV130. **f** Geometric Mean Fluorescence Intensity (GeoMFI) values for CD40 (Ctrl- $n = 3$-4, MV130 $n = 4$-5, Gefinitib/MV130 $n = 5$ biological replicates; 1 independent experiment). **g** Cytokine production in cell-free supernatants after in vitro stimulation of wild type and MyD88$^{-/-}$ BMDCs for 18 h (Ctrl- $n = 3$-4, MV130 $n = 4$-5, Gefinitib/MV130 $n = 7$ biological replicates; 1 independent experiment). **h** Serum total IgE and HDM specific IgG1 levels ($n = 4$ mice per group). **i** Quantification of total cell numbers and **j** different cell types in BALF determined by flow cytometry ($n = 4$ mice per group). Values are mean ± SEM. Statistical significance was determined using unpaired One-way ANOVA (**b**, **c** and **i**), unpaired Two-way ANOVA (**f** and **g**) and two-side unpaired Student's $t$ test (**d** and **j**): $^{*}p < 0.05$, $^{**}p < 0.01$, $^{***}p < 0.001$ and $^{****}p < 0.0001$. Exact $p$ values and source data are available in the Source Data file.

alternative mouse strains and allergen models are warranted to strengthen and generalize these findings.

To verify that MV130 could also promotes proper immune responses against HDM in humans, we studied its capacity to immunomodulate human DCs as key cells involved in linking innate and adaptive immune responses[3,4]. We showed that MV130 + HDM-stimulated human DCs from both healthy and HDM-allergic asthma donors produced higher TNF-α, IL-6 and IL-10 than human DCs stimulated with HDM alone. MV130 also generated human DCs from both healthy and allergic asthma donors able to inhibit HDM-induced Th2 polarization and to enhance Th1 and IL-10-producing T cells. Supporting these data our GSEA showed that TNF-α-, IFN-γ-, IL-6- and IL-10-mediated pathways are significantly enriched in MV130-stimulated human DCs from healthy donors. It has been also shown that the in vivo anti-allergic properties of *Acinetobacter lwoffii* is mediated by local production of IL-6 in the airways leading to the generation of IL-10-producing T cells[18]. Deeper analysis of genes included in MV130-stimulated human DCs enriched data sets, reveals an enrichment in TNFAIP3 (also known as A20), a gene highly associated with the "farm protective effect" for asthma and reported downregulated in asthmatic children[37,40]. Remarkably, GSEA also uncovered gene set enrichments associated to the mTOR and glycolysis pathways in MV130-stimulated human DCs and gene set enrichment associated to OXPHOS pathways within unstimulated DCs, suggesting that MV130 induces metabolic reprogramming in human DCs that might be linked to the restoration of non-pathological immune responses against HDM. It has been previously shown that rFlaA:Betv1 immunomodulatory functions on DCs is mediated by the mTOR-dependent metabolic switch to glycolysis, which is connected to DCs' cytokine production of IL-6, IL-12, TNF-α and IL-10, and to the inhibition of T2 allergic responses[56]. Our in vitro metabolic experiments, including real-time metabolic assays in a Seahorse analyser, confirmed that MV130 enhanced glycolysis and reduced OXPHOS in human DCs, which is sustained upon HDM stimulation. In line with our human DCs in vitro experiments, in vivo i.n. administration of MV130-stimulated BMDCs inhibited T2 pathological responses against HDM and prevented allergic sensitization and eosinophilic airway inflammation by mechanisms partially depending on MyD88-mediated signalling pathways. All these results highlight the key role played by DCs in the reported anti-allergic and anti-asthmatic effects of MV130 both in mice and humans.

In conclusion, MV130 may not only protect against respiratory viruses, but also prevent allergic sensitization and eosinophilic asthma by modulating innate and adaptive immune responses to HDM. Our findings suggest that MV130 is a promising mucosal vaccine with the potential to reduce the risk of allergic asthma development. Clinical trials to confirm its safety and efficacy in this indication are warranted.

## Methods

### Ethics statement

All mice procedures included in this study were reviewed and ethically approved by Universidad Complutense de Madrid (UCM) and Comunidad Autónoma de Madrid (CAM) within the context of project IND2019/BMD17182 from CAM and PID2020-114396RB-I00 from Ministerio de Ciencia e Innovación (Spain) to O.P. under PROEX 152/18, PROEX3221.1/21 from CAM. Blood samples from adult healthy donors (>18 years old; 54% male and 46% female) were obtained from the Transfusion Centre of Madrid (approved by CAM; approval reference: PO.DIS.09). Blood samples from 6 adults moderate-to-severe HDM-allergic asthmatic patients (>18 years old; 50% male and 50% female) were obtained from Lucus Augusti University Hospital (approved by the local ethics committee for drugs research of Galicia (CEIm-G) and Lucus Augusti University Hospital; approval reference: Pneu-01-2025). All participants in this study signed informed consent documents, and the data were treated according to recommended criteria of confidentiality, following the ethical guidelines of the 1975 Declaration of Helsinki.

### Media and reagents

RPMI 1640 (Lonza) supplemented with 10% foetal bovine serum (FBS), 100 μg/mL normocin (InvivoGen), 50 μg/mL penicillin/streptomycin, 1% non-essential aminoacids, 1% MEM vitamins and 1 mM sodium pyruvate (all from Life Technologies) (cRPMI). Polybacterial preparation, MV130 composed of whole heat-inactivated bacteria (60% V104 *S. pneumoniae*, 15% V102 *S. aureus*, 15% V101*S. epidermidis*, 4% V113 *K. pneumoniae*, 3% V105 *M. catarrhalis* and 3% V103 *H. influenzae*), House Dust Mites (HDM, *Dermatophagoides pteronyssinus*) extract and 0.1% NaCl vehicle were provided by Inmunotek S.L. (Der p 1: 40,58 μg/mL; Der p 2: 8,42 μg/mL; LPS: 2EU/μg).

### Animals

C57BL/6J female mice (6–8 weeks) were obtained from Charles River, and Myd88$^{-/-}$ C57BL/6J mice (B6.129P2(SJL)-Myd88tm1.1Defr/J mice) from Jackson Laboratory. All animals were acclimatized for 1 week before experiments and housed in a specific pathogen-free environment at 20–24 °C and 45–55% humidity with a 12 h light-dark cycle and permitted ad libitum consumption of water and a standard chow diet (hybridpellet, Altromin) at the Animal Facility Unit at UCM.

### Mice asthma models

Acute HDM asthma model was developed in C57BL/6J female mice (6–8 weeks; Charles River) by intranasal (i.n.) administration of 1 μg of HDM (Inmunotek S.L.) on day 1 and subsequently i.n. challenges with 10 μg of HDM on days 8–12[25]. As shown in Supplementary Fig. 7, this is a well-established HDM asthma model where the first HDM i.n. administration is essential to induce allergen sensitization, which is indispensable to mount HDM-specific IgE responses and HDM-mediated eosinophilic airway inflammation upon the subsequent HDM challenges. On days 2–4, mice were i.n. treated with 50 μL of MV130 at 300 FTU (approx.$10^9$ bacteria/mL; therefore, approx. 5 ×107 bacteria/day; Inmunotek S.L) or vehicle (0.1% NaCl). MV130 dose was selected based on published studies demonstrating efficacy to protect against viral respiratory infections in mice[21] and initial pilot studies assessing the capacity to prevent eosinophilic infiltration in BALF. Three days after the last HDM-challenge lung function was measured, mice were sacrificed and blood, bronchoalveolar lavage fluid (BALF), lungs, mediastinal lymph nodes (MLNs) and spleen were collected. For type 2 innate lymphoid cells (ILC2s) studies, mice were sacrificed one day after the last HDM-challenge. A non-treated group receiving PBS during sensitization and challenge was also included as a control group (PBS group). A control group receiving MV130 alone at days 2–4 without sensitization or challenge was also included as a control group (MV130 group).

For MV130 prophylactic experiments, C57BL/6J female mice (6–8 weeks; Charles River) were i.n. administered with 50 μL of vehicle (HDM group) or with 50 μL of MV130 at 300 FTU (approx.$10^9$ bacteria/ml; therefore, approx. 5 ×107 bacteria/day; Inmunotek S.L) (MV130-HDM group) for 3 consecutive days for 2 weeks and then left resting for 1, 2, 4 or 9 weeks prior to HDM sensitization following our conventional protocol (one single dose of HDM for sensitization followed by 5 consecutive challenges with the allergen during the following week) (Fig. 5a). As controls, we included one group receiving only PBS during the whole protocol (PBS group) and another group receiving prophylactic MV130 alone without subsequent HDM- sensitization/challenge (MV130 group).

### Mouse lung function measurements

Mouse airway hyperresponsiveness (AHR) was measured 72 h after the last HDM challenge with aerosolized methacholine chloride (Mch) (Sigma) using two different techniques. In conscious unrestrained mice, lung function was measured by whole-body plethysmography (WBP) (BUXCO Electronics Ltd.). PBS, followed by increasing concentrations of Mch (6.25, 12.5 and 25 mg/ml) were nebulized, and lung function was recorded for 3 min, and enhanced pause (Penh) was

calculated using FinePoint software (BUXCO Electronics Ltd.), which is a dimensionless unit that correlates with bronchoconstriction. Airway resistance (Resistance index, RI) was measured in anesthetized mice with ketamine/medetomidine (75/1 mg/kg, intraperitoneally, i.p) and tracheostomized with an 18-gauge metal cannula inserted into the trachea, preventing air leakage by tightly tied suture thread. The cannula was connected to a computer-connected mechanical ventilator of Resistance and Compliance System (R&D, BUXCO Electronics Ltd.). PBS followed by increasing concentrations of methacholine (12.5, 25 and 50 mg/mL) were nebulized and lung function was recorded for 3 min. RI ($cmH_2O/mL/s$) was calculated using FinePoint software (BUXCO Electronics Ltd.).

### Serum collection

Mice were anaesthetised with isoflurane and peripheral blood was collected via retro-orbital bleeding using lime glass Pasteur pipettes and microtainer tubes (Beckton Dickinson). Samples were centrifuged at 1000 × *g* for 10 min at room temperature. Serum was collected and stored at −80 °C for further analysis.

### Immunoglobulin measurement

Mouse total IgE and HDM-specific antibodies were measured by enzyme-linked immunosorbent assay (ELISA) in mouse serum. Total IgE was measured using a commercial ELISA kit (BD Biosciences) following manufacturer's protocol. HDM-specific IgE and IgG1 were measured by ELISA. High binding 96-well plates (Corning) were coated with HDM (50 µg/mL) in coating buffer overnight (ON) at 4 °C. Coated plates were blocked with 10% FBS in PBS for 2 h at room temperature. Plates were washed and incubated with serum samples ON at 4 °C. After washing, rat anti-mouse IgE-HRP (Southern Biotech) or goat anti-mouse IgG1-HRP (Thermo Fisher Scientific) were added and incubated for 2 h at room temperature. O-phenyldiamine (OPD) was used to develop the assay, and $H_2SO_4$ was added to stop the reaction for absorbance reading at 492 nm.

### Bronchoalveolar fluid isolation, cell population analysis and epithelial assays

BALF isolation was performed, 24 h (for ILC2s and albumin studies) or 72 h (for the rest of analysis) after the last HDM-challenge by 3 consecutive flushes of the airways through catheterized trachea with 700 µL of ice-cold 10 mM EDTA in PBS. The first flush of the airways was obtained separately and centrifuged (300 × *g*, 10 min) to obtain BALF supernatant. BALF supernatant was stored at −80 °C for future analysis, and cell pellets were added to the rest of the BALF. Cells were counted by Trypan blue exclusion by light microscope and cells were washed in PBS/EDTA (2 mM) 0.5% BSA. Cell profile was determined by flow cytometry with a specific antibody cocktail (Supplementary Table 1). The gating strategy for cell populations in BALF is shown in Supplementary Fig. 1.

Epithelial damage was assessed by determining lactate dehydrogenase (LDH) activity in BALF using CyQUANT LDH Cytotoxicity Assay Kit (Fisher), following manufacturer's protocols. Bronchial epithelial leakage to the airway lumen was assessed by measuring BSA concentration in BALF using an albumin ELISA kit (Abcam), following manufacturer's protocols. Eosinophil peroxidase (EPX) activity in BALF was measured by OPD substrate oxidation by EPX in the presence of $H_2O_2$ at 37 °C pH 8 protected for light for 30 min. $H_2SO_4$ was added to stop the reaction; absorbance was measured at 492 nm.

### Lung isolation and processing

The lungs from mice that were not used for BALF isolation were perfused with 10 mL of ice-cold PBS through the right ventricle. After perfusion, lungs were isolated aseptically and cut into small pieces before enzyme digested for 1 h at 37 °C in PBS containing Liberase TL (Roche) and DNase I (Roche) to obtain a single-cell suspension. Cell suspensions were rinsed with ice-cold FBS to stop enzyme digestion and passed through a 70 µm nylon cell strainer. Cells were counted by Trypan blue exclusion by light microscope and different cell populations were analysed by flow cytometry with a specific antibody cocktail (Supplementary Table 1). The gating strategies were detailed in Supplementary Fig. 2, and Supplementary Fig. 3a, b, 3d, for eosinophil, T cell and ILC2 subsets, respectively.

### Lung histology

Left lungs from mice that were not used for BALF isolation were isolated aseptically and immediately fixed in 4% paraformaldehyde for 48 h. Afterwards, lungs were washed five times with PBS, embedded in paraffin and sectioned (5-µm thick) for future analysis.

Lung sections were deparaffinized and stained with haematoxylin and eosin (H&E) to evaluate airway inflammation, periodic acid-Schiff (PAS) to analyse mucus, and modified Highman's Congo Red to analyse eosinophils, following conventional methods. Immunohistochemistry was used to detect α-smooth muscle actin (α-SMA) to assess smooth muscle thickening. H&E, PAS, α-SMA and Congo Red lung staining were digitalized. Ten medium size airways per mice were analysed for H&E, PAS, α-SMA quantification with Zen Blue and ImageJ software.

For major basic protein (MBP) and EPX immunofluorescence staining, lung sections were deparaffinized and antigens were retrieved with pepsin solution Digest-All™ 3 at 37 °C for 10 min (Life technologies). Sections were blocked with 3% BSA, 0.1% TRITON in PBS at room temperature for 1 h and then, stained with primary antibodies ON at 4 °C (1:500, rat anti-mouse-MBP, MT2-14.7.3, and 1:500, mouse-anti-mouse monoclonal-EPX, MM25-82.2.1) (Mayo Clinic). After washing with 0.1% TRITON in PBS, secondary antibodies (1:200, goat anti-rat Alexa Fluor 555, Invitrogen and 1:200 goat anti-mouse-A488, Invitrogen) were added for 45 min, protected from light at room temperature. After washing with 0.1% TRITON in PBS, sections were incubated for 10 min at room temperature with Hoechst for nuclear staining. Finally, following washing steps with PBS, sections were mounted with Prolon™Gold (Invitrogen) for future analysis. Immunofluorescence images were obtained with THUNDER Imager 3D Tissue for quantification of all lungs and with Olympus confocal microscope FV1200 for high resolution images at 20× and 40× magnifications. MBP and EPX quantification was carried out with ImageJ software by measuring the area ($\mu m^2$) of MBP or EPX staining on a total of 15 and 13 fields, respectively, /$\mu m^2$ of lung in the field ×100.

### MLNs processing

MLNs were isolated aseptically, minced between frosted slides in RPMI medium, and filtered through 40 µm nylon cell strainers to obtain a single-cell suspension. Cells were counted by Trypan blue exclusion by light microscope and DC subsets were determined by flow cytometry with a specific antibody cocktail (Supplementary Table 1). The gating strategy was detailed in Supplementary Fig. 3c.

### Spleen processing and splenocyte culture

Spleens were isolated aseptically, minced, and filtered through a 40 µm nylon cell strainers to obtain a single-cell suspension. Then, red blood cells were lysed with ACK lysis buffer before being resuspended in cRPMI and assessing splenocyte viability. Triplicates of 0.8 ×106 splenocytes of each group of mice were cultured with HDM (100 µg/mL) in 96-well flat-bottom plates (Corning). After 3 days of culture at 37 °C and 5% $CO_2$, triplicates were pooled and cell-free supernatants were used to quantify IL-13, IL-5, IL-10 and IFN-ɣ cytokines by ELISA.

### RNA isolation, cDNA synthesis, and quantitative PCR

For lung mRNA expression, a portion of 20–30 mg from the right lung was harvested, snap-frozen in liquid nitrogen and stored at −80 °C. Afterwards, samples were disrupted in liquid nitrogen with a pestle and immediately homogenized in lysis buffer (RNeasy Mini Kit,

Qiagen). Then, RNA from lysed samples was isolated with RNeasy Mini Kit according to the manufacturer's protocol. Complementary DNA was generated with a PrimeScript RT Reagent Kit (Takara Bio). Finally, quantitative PCR (qPCR) was performed by using FastStart Universal SYBR Green Master (Roche). The sequences of the primer pairs used are the following: *Occludin* (forward: ACAAGAGAAATTTTGATGCAGGTCT, reverse: CATCAGCAGCAGCCATGTACTC), *Tjp1* (*Zo-1*)(forward: GGAGATGTTTATGCGGACGG, reverse: CCATTGCTGTGCTCTTAGCG). *Eef1a1* (forward: CGGCAGTCGCCTTGGACGTT, reverse: CGGTGGTTTTCACAACACCTGCGT) was employed as a housekeeping gene.

### BMDCs generation, in vitro and in vivo experiments

BMDCs from wild type or Myd88$^{-/-}$ C57BL/6J mice (6–8 weeks; Charles River) were generated from bone marrow progenitors[57], which were flushed out of the femur and tibia, processed and cultured in cRPMI with mouse GM-CSF (20 ng/mL; Peprotech) for 8–10 days until complete differentiation. For in vitro experiments BMDCs (WT or Myd88$^{-/-}$) were stimulated for 18 h at 37 °C and 5% $CO_2$ with vehicle, MV130 or MV130 in the presence of RIPK2 inhibitor Gefitinib (10 μM, InvivoGen). Cell surface marker expression and cytokine production were analysed by flow cytometry and ELISA, respectively. For in vivo adoptive transfer experiments, on day 8–10 of the differentiation, BMDCs (WT or Myd88$^{-/-}$) were stimulated with vehicle (Vehicle-BMDCs) or MV130 (MV130-BMDCs) for 18 h at 37 °C and 5% $CO_2$. Then, vehicle- and MV130-stimulated BMDCs were harvested, washed and intranasally transferred into wildtype C57BL6/J mice ($10^6$ cells/50 μL of PBS per mouse) 8 h prior to mice sensitization to generate a Vehicle-BMDCs/HDM group and a MV130-BMDCs/HDM group, respectively. A group receiving PBS administration in the treatment, sensitization and challenge was included as a control. Three days after the last HDM-challenge mice were sacrificed and blood and BALF were collected.

### Peripheral blood mononuclear cells isolation and human-monocyte-derived dendritic cells generation

PBMCs were obtained by FicollPaque Plus (GE-Healthcare) density gradient centrifugation. Immature HmoDCs were generated from blood monocytes obtained from total PBMC using anti-CD14 microbeads (Miltenyi Biotec) and autoMACs Pro (Miltenyi Biotec) and cultured for 6 days with cRPMI medium containing 100 ng/mL of IL-4 and GM-CSF (PeproTech). The purity and phenotype of monocytes and generated immature HmoDCs were analysed by flow cytometry with lineage-specific markers.

### Human cell cultures and co-culture experiments

PBMCs from healthy donors ($10^6$ cells/mL) were stimulated with vehicle (Ctrl-), HDM (100 μg/mL) or HDM + MV130 (100 μg/mL/ 3 FTU [approx.$10^7$ bacteria/mL]) for 4 days at 37 °C and 5% $CO_2$. IL-2 (20 ng/mL) was included in all conditions. Cell-free supernatants were used to IL-10, IL-6, IL-5 and IFN-ɣ quantification by ELISA.

Immature HmoDCs ($10^6$ cells/mL) from healthy or HDM-allergic asthmatic donors were stimulated with vehicle (Ctrl-), HDM (100 μg/mL), MV130 (3 FTU [approx.$10^7$ bacteria/mL]) or HDM + MV130 (100 μg/mL/ 3 FTU [approx.$10^7$ bacteria/mL]) for 24 h at 37 °C and 5% $CO_2$. Cell-free supernatants were used for TNF-α, IL-6 and IL-10 cytokine quantification by ELISA, and cell pellets were employed for metabolic assays.

For co-culture experiments, naïve CD4$^+$ T cells were isolated from PBMC using the "Naïve CD4$^+$ T Cell Isolation Kit" (Miltenyi Biotec) and autoMACS Pro, according to manufacturer protocol. Immature HmoDCs were co-cultured with purified allogenic naïve CD4$^+$ T cells (1:5 DC/T cell) for 3 days in the presence of vehicle (Ctrl-), HDM (100 μg/mL) or HDM + MV130 (100 μg/mL/ 3 FTU [approx.$10^7$ bacteria/mL]) at 37 °C and 5% $CO_2$. Cell-free supernatants were used to IFN-ɣ, IL-5 and IL-10 quantification by ELISA.

### Gene array gene set enrichment analysis (GSEA)

Gene array data set of MV130- or vehicle (Ctrl-)-stimulated HmoDCs for 24 h were obtained from Expression Atlas repository (https://wwwdev.ebi.ac.uk/gxa/experiments/E-MTAB-5259/Results) from our previous work[21]. Gene set enrichment analysis (GSEA) was performed using the GSEA program (http://software.broadinstitute.org/gsea/index.jsp). GSEA was used to identify HALLMARK, Gene Ontology Biological Process (GOBP), BIOCARTA and Kyoto Encyclopaedia of Genes and Genomes (KEGG) gene sets from the Molecular Signatures database (MSigDB) that were significantly enriched in MV130 or vehicle (Ctrl-) phenotype. Other graphical representations (bar plots) apart from GSEA classic representations were produced with GraphPad Prism software, 8.0 version.

### Metabolic studies

Real-time metabolic profiling of HmoDCs was performed using a Seahorse XF HS Mini Analyzer (Agilent). HmoDCs were stimulated 24 h with vehicle (Ctrl-), HDM (100 μg/mL), MV130 (3 FTU [approx.$10^7$ bacteria/mL]) or HDM + MV130 (100 μg/mL/ 3 FTU [approx.$10^7$ bacteria/mL)] at 37 °C and 5% $CO_2$. After stimulation, cells were washed and cultured with XF DMEM medium supplemented with 10 mM glucose, 1 mM pyruvate and 2 mM glutamine in poly-D-lysine-coated 8-well miniplates in a $CO_2$-free incubator for 1 h at 37 °C before the assay. To accurately monitor glycolysis, we analysed the glycolytic proton efflux rate (glycoPER) at three consecutive stages: basal conditions (no drugs administrated), inhibition of the electron transport chain (0.5 μM Rotenone (Rot) and 0.5 μM Antimycin A (AA)) and inhibition of glycolysis (50 mM 2-deoxy-D-glucose (2-DG)) (Sigma-Aldrich). Seahorse-derived data were analysed using Agilent Seahorse Analytics.

Mitochondrial membrane potential and mitochondrial mass were measured after 24 h of HmoDCs stimulation with the mentioned stimulus using MitoTracker™ Red CMXRos and MitoTracker™ Green FM (all from ThermoFisher Scientific), respectively, following the manufacturer's instructions with minor modifications. The fluorescence of the probes was analysed using FLUOstar OPTIMA fluorescence reader (BMG LabTech).

### Cytokine quantification

Human TNF-α, IL-6, IL-10, IL-5, and IFN-ɣ, and murine IL-5, IFN-ɣ in cell-free supernatants were quantified by ELISA cytokine kits from BD Biosciences. Murine IL-10 and IL-13 levels were assessed in cell-free supernatants by ELISA using specific kits from Invitrogen and R&D System, respectively. In all cases, the manufacturer's protocols were followed with minor modifications.

### Flow cytometry

For surface stains, cells were washed with PBS/EDTA (2 mM) 0.5% BSA and labelling of cell-surface markers was performed at room temperature for 15 min for human samples or at 4 °C for 30 min for mouse samples protected from light with fluorescence-labelled antibodies (Supplementary Table 1). After staining, cells were fixed in 0.1% PBS/PFA for flow cytometry analysis. The gating strategies are detailed in Supplementary Figs. 1–3c.

For intracellular cytokine staining, lung isolated cells were washed and restimulated with 25 ng/mL PMA plus 1 mg/mL ionomycin (6 h for T cells and 4 h for ILC2s) and 10 mg/mL Brefeldin A (last 4 h for T cells and last 3 h for ILC2s). After surface staining at 4 °C for 30 min protected from light with fluorescence-labelled antibodies (Supplementary Table 1), cells were fixed and permeabilized with Cytofix/Cytoperm (BD Biosciences) according to the manufacturer's instructions. The cells were intracellular stained with the combination of fluorochrome-labelled antibodies (Supplementary Table 1). Cells were fixed in 1% PBS/PFA for flow cytometry analysis. The gating strategy is detailed in Supplementary Fig. 3a, d.

For FOXP3 intracellular staining, after surface staining, cells were fixed and permeabilized with FOXP3 Fix/Perm buffer for 20 min protected from light at room temperature (Supplementary Table 1). A second permeabilization was carried out with FOXP3 Perm buffer for 15 min in darkness at room temperature. Then, cells were stained with Alexa Fluor 488 anti-mouse FOXP3 for 30 min in darkness at room temperature. Cells were fixed in 1% PBS/PFA for flow cytometry analysis. The gating strategy is detailed in Supplementary Fig. 3b. Fixed cells were analysed in the FACS Aria III or FACSymphony A1 cytometers (Beckton Dickinson) in the Flow Cytometry and Fluorescence Microscopy Unit at Complutense University of Madrid. Flow cytometry data were analysed using FlowJo V10 software.

### Statistical analysis

Mice were included in the studies in a blind manner and randomly assigned to receive only saline (PBS group), vehicle (HDM group), MV130 without sensitization (MV130 group) or MV130 with sensitization (HDM + MV130 group). Normal distribution of data was evaluated using the Shapiro–Wilk test. Statistical analyses were performed using GraphPad Prism software, 8.0 version. All the data were expressed as mean ± SEM of the corresponding parameter. Parametric statistical analyses were calculated using paired or unpaired One-way ANOVA, Two-way ANOVA or Student's *t* test. Nonparametric analyses were calculated using paired or unpaired Kruskal–Wallis, Mann–Whitney *U* test, Wilcoxon test and Welch's *t* test. Correlations were performed by Pearson's parametric correlation test. Differences were considered statistically significant when $p < 0.05$. For all figure panels, *p*-values are provided as a Supplementary Data file.

### Reporting summary

Further information on research design is available in the Nature Portfolio Reporting Summary linked to this article.

## Data availability

All data generated in this study are provided in the Source Data file. Source data are provided with this paper.

## References


1. Venkatesan, P. 2023 GINA report for asthma. *Lancet Respir. Med.* **11**, 589 (2023).
2. Agache, I. et al. EAACI biologicals guidelines-recommendations for severe asthma. *Allergy* **76**, 14–44 (2021).
3. Kolkhir, P. et al. Type 2 chronic inflammatory diseases: targets, therapies and unmet needs. *Nat. Rev. Drug Discov.* **22**, 743–767 (2023).
4. Akdis, C. A. et al. Type 2 immunity in the skin and lungs. *Allergy* **75**, 1582–1605 (2020).
5. Wenzel, S. E. Asthma phenotypes: the evolution from clinical to molecular approaches. *Nat. Med.* **18**, 716–25 (2012).
6. Agache, I. & Akdis, C. A. Precision medicine and phenotypes, endotypes, genotypes, regiotypes, and theratypes of allergic diseases. *J. Clin. Invest.* **129**, 1493–1503 (2019).
7. Komlosi, Z. I. et al. Cellular and molecular mechanisms of allergic asthma. *Mol. Asp. Med.* **85**, 100995 (2022).
8. Roan, F., Obata-Ninomiya, K. & Ziegler, S. F. Epithelial cell-derived cytokines: more than just signaling the alarm. *J. Clin. Invest.* **129**, 1441–1451 (2019).
9. Kemter, A. M. & Nagler, C. R. Influences on allergic mechanisms through gut, lung, and skin microbiome exposures. *J. Clin. Invest.* **129**, 1483–1492 (2019).
10. Jackson, D. J., Gern, J. E. & Lemanske, R. F. Jr., The contributions of allergic sensitization and respiratory pathogens to asthma inception. *J. Allergy Clin. Immunol.* **137**, 659–65 (2016).
11. Rubner, F. J. et al. Early life rhinovirus wheezing, allergic sensitization, and asthma risk at adolescence. *J. Allergy Clin. Immunol.* **139**, 501–507 (2017).
12. Martin-Cruz, L. et al. From trained immunity in allergy to trained immunity-based allergen vaccines. *Clin. Exp. Allergy* **53**, 145–155 (2023).
13. Esposito, S. et al. Nonspecific immunomodulators for recurrent respiratory tract infections, wheezing and asthma in children: a systematic review of mechanistic and clinical evidence. *Curr. Opin. Allergy Clin. Immunol.* **18**, 198–209 (2018).
14. Nieto, A. et al. Bacterial mucosal immunotherapy with MV130 prevents recurrent wheezing in children: a randomized, double-blind, placebo-controlled clinical trial. *Am. J. Respir. Crit. Care Med.* **204**, 462–472 (2021).
15. Sanchez-Ramon, S. et al. Trained immunity-based vaccines: a new paradigm for the development of broad-spectrum anti-infectious formulations. *Front Immunol.* **9**, 2936 (2018).
16. Marques Dos Santos, M. et al. Asthma-protective agents in dust from traditional farm environments. *J. Allergy Clin. Immunol.* **152**, 610–621 (2023).
17. Vercelli, D. From Amish farm dust to bacterial lysates: the long and winding road to protection from allergic disease. *Semin. Immunol.* **68**, 101779 (2023).
18. Alashkar Alhamwe, B. et al. Intranasal administration of Acinetobacter lwoffii in a murine model of asthma induces IL-6-mediated protection associated with cecal microbiota changes. *Allergy* **78**, 1245–1257 (2023).
19. Pivniouk, V. et al. Airway administration of OM-85, a bacterial lysate, blocks experimental asthma by targeting dendritic cells and the epithelium/IL-33/ILC2 axis. *J. Allergy Clin. Immunol.* **149**, 943–956 (2022).
20. Cirauqui, C. et al. Human dendritic cells activated with MV130 induce Th1, Th17 and IL-10 responses via RIPK2 and MyD88 signalling pathways. *Eur. J. Immunol.* **48**, 180–193 (2018).
21. Brandi, P. et al. Trained immunity induction by the inactivated mucosal vaccine MV130 protects against experimental viral respiratory infections. *Cell Rep.* **38**, 110184 (2022).
22. Nieto, A. et al. Do bacterial vaccines/adjuvants prevent wheezing episodes in children? *Curr. Opin. Allergy Clin. Immunol.* **22**, 380–386 (2022).
23. Krishnamoorthy, N. et al. Early infection with respiratory syncytial virus impairs regulatory T cell function and increases susceptibility to allergic asthma. *Nat. Med.* **18**, 1525–30 (2012).
24. Mehta, A. K. et al. Rhinovirus infection interferes with induction of tolerance to aeroantigens through OX40 ligand, thymic stromal lymphopoietin, and IL-33. *J. Allergy Clin. Immunol.* **137**, 278–88.e6 (2016).
25. Willart, M. A. et al. Interleukin-1alpha controls allergic sensitization to inhaled house dust mite via the epithelial release of GM-CSF and IL-33. *J. Exp. Med.* **209**, 1505–17 (2012).
26. Boonpiyathad, T. et al. Immunologic mechanisms in asthma. *Semin. Immunol.* **46**, 101333 (2019).
27. Hammad, H. & Lambrecht, B. N. The basic immunology of asthma. *Cell* **184**, 1469–1485 (2021).
28. Saunders, R. et al. DP(2) antagonism reduces airway smooth muscle mass in asthma by decreasing eosinophilia and myofibroblast recruitment. *Sci. Transl. Med.* **11**, eaao6451 (2019).
29. Dunican, E. M. et al. Mucus plugs in patients with asthma linked to eosinophilia and airflow obstruction. *J. Clin. Invest.* **128**, 997–1009 (2018).
30. Mesnil, C. et al. Lung-resident eosinophils represent a distinct regulatory eosinophil subset. *J. Clin. Invest.* **126**, 3279–95 (2016).
31. Wechsler, M. E. et al. Eosinophils in health and disease: a state-of-the-art review. *Mayo Clin. Proc.* **96**, 2694–2707 (2021).

32. Sugita, K. et al. Type 2 innate lymphoid cells disrupt bronchial epithelial barrier integrity by targeting tight junctions through IL-13 in asthmatic patients. *J. Allergy Clin. Immunol.* **141**, 300–310 e11 (2018).
33. Steelant, B. et al. Histamine and T helper cytokine-driven epithelial barrier dysfunction in allergic rhinitis. *J. Allergy Clin. Immunol.* **141**, 951–963 e8 (2018).
34. Drent, M. et al. Usefulness of lactate dehydrogenase and its isoenzymes as indicators of lung damage or inflammation. *Eur. Respir. J.* **9**, 1736–42 (1996).
35. Martin-Cruz, L. et al. A tumor-associated heparan sulfate-related glycosaminoglycan promotes the generation of functional regulatory T cells. *Cell Mol. Immunol.* **20**, 1499–1512 (2023).
36. Subramanian, A. et al. Gene set enrichment analysis: a knowledge-based approach for interpreting genome-wide expression profiles. *Proc. Natl. Acad. Sci. USA* **102**, 15545–50 (2005).
37. Krusche, J. et al. TNF-alpha-induced protein 3 is a key player in childhood asthma development and environment-mediated protection. *J. Allergy Clin. Immunol.* **144**, 1684–1696.e12 (2019).
38. Dawicki, W. et al. CD40 signaling augments IL-10 expression and the tolerogenicity of IL-10-induced regulatory dendritic cells. *PLoS One* **16**, e0248290 (2021).
39. Busse, W. W., E. Melen, E. & Menzies-Gow, A. N. Holy Grail: the journey towards disease modification in asthma. *Eur. Respir. Rev.* **31**, 210183 (2022).
40. Renz, H. & Skevaki, C. Early life microbial exposures and allergy risks: opportunities for prevention. *Nat. Rev. Immunol.* **21**, 177–191 (2021).
41. Deckers, J., Marsland, B. J. & von Mutius, E. Protection against allergies: microbes, immunity, and the farming effect. *Eur. J. Immunol.* **51**, 2387–2398 (2021).
42. Barcik, W. et al. The role of lung and gut microbiota in the pathology of asthma. *Immunity* **52**, 241–255 (2020).
43. Salehian, S. et al. Phenotype and endotype based treatment of preschool wheeze. *Expert Rev. Respir. Med.* **17**, 853–864 (2023).
44. Del Fresno, C. et al. The bacterial mucosal immunotherapy MV130 protects against SARS-CoV-2 infection and improves COVID-19 vaccines immunogenicity. *Front. Immunol.* **12**, 748103 (2021).
45. Thanasarnthungcharoen, C. et al. Immunotherapeutic effects of specific and nonspecific mRNA-lipid nanoparticles in a mouse model of HDM-induced airway inflammation. *Allergy* **79**, 1974–1978 (2024).
46. Duechs, M. J. et al. Development of a novel severe triple allergen asthma model in mice which is resistant to dexamethasone and partially resistant to TLR7 and TLR9 agonist treatment. *PLoS One* **9**, e91223 (2014).
47. Pfaar, O. et al. One hundred ten years of allergen immunotherapy: a broad look into the future. *J. Allergy Clin. Immunol. Pr.* **9**, 1791–1803 (2021).
48. Lin, Y. J., Zimmermann, J. & Schulke, S. Novel adjuvants in allergen-specific immunotherapy: where do we stand? *Front. Immunol.* **15**, 1348305 (2024).
49. Shamji, M. H. et al. The role of allergen-specific IgE, IgG and IgA in allergic disease. *Allergy* **76**, 3627–3641 (2021).
50. Palomares, O. et al. dIvergEnt: how IgE axis contributes to the continuum of allergic asthma and anti-IgE therapies. *Int. J. Mol. Sci.* **18**, 1328 (2017).
51. Lopez-Abente, J. et al. Omalizumab restores the ability of human plasmacytoid dendritic cells to induce Foxp3(+)Tregs. *Eur. Respir. J.* **57**, 2000751 (2021).
52. Benito-Villalvilla, C. et al. Ligelizumab impairs IgE-binding to plasmacytoid dendritic cells more potently than omalizumab and restores IFN-alpha production and FOXP3(+) Treg generation. *Allergy* **78**, 1060–1072 (2023).
53. Akdis, C. A. Does the epithelial barrier hypothesis explain the increase in allergy, autoimmunity and other chronic conditions? *Nat. Rev. Immunol.* **21**, 739–751 (2021).
54. Heijink, I. H. et al. Epithelial cell dysfunction, a major driver of asthma development. *Allergy* **75**, 1902–1917 (2020).
55. Kim, S. R. Viral infection and airway epithelial immunity in asthma. *Int. J. Mol. Sci.* **23**, 9914 (2022).
56. Schulke, S. et al. Critical role of mammalian target of rapamycin for IL-10 dendritic cell induction by a flagellin A conjugate in preventing allergic sensitization. *J. Allergy Clin. Immunol.* **141**, 1786–1798.e11 (2018).
57. Dong, Y. et al. Generation and identification of GM-CSF derived alveolar-like macrophages and dendritic cells from mouse bone marrow. *J. Vis. Exp.* **112**, 54194 (2016).


## Acknowledgements

This work was supported by grant IND2019/BMD17182 to O.P. from the Industrial Doctoral Program (UCM-Inmunotek S.L) from Comunidad Autónoma de Madrid (CAM). C.S.-O. was contracted with this grant by Inmunotek SL to perform her Doctoral Thesis in UCM. O.P. laboratory is also supported by grant PID2020-114396RB-I00 from MICINN, Spain. Work in the lab of F.X.R. was supported, in part, by grant PID2021-128125OB-I00 from Ministerio de Ciencia, Innovación y Universidades (Madrid, Spain) (co-funded by the ERDF-EU). CNIO is supported by Ministerio de Ciencia, Innovación y Universidades as a Centro de Excelencia Severo Ochoa SEV-2015-0510." A.G. is recipient of a predoctoral fellowship from AECC.

## Author contributions

Conceived and designed the study: O.P. Performed the experiments: C.S.-O., A.A., L.M.-C., M.P.-D., A.M., B.L., B.M.-R. and A.G. Provided reagents and logistics: L.P.LL., L.C., J.L.S., F.X.R., and O.P. Analysed and discussed the data: C.S.-O., A.A., L.M.-C., M.P.-D., A.M., L.C., J.L.S. and O.P. Wrote the paper: O.P. and C.S.-O. All the authors revised the manuscript, contributed with discussions and revisions and approved the final version of the manuscript.

## Competing interests

O.P. received research grants from MINECO, Ministerio de Ciencia e Innovación, Inmunotek S.L., Novartis, and AstraZeneca and fees for giving scientific lectures or participation in Advisory Boards from: AstraZeneca, Pfizer, GlaxoSmithKline, Inmunotek S.L, Novartis, Sanofi-Genzyme and Regeneron. J.L.S. is the founder and CEO of Inmunotek SL and C.S.-O. and L.C. are employees of Inmunotek S.L. The rest of authors have no conflict of interest to declare.

## Additional information

**Supplementary information** The online version contains supplementary material available at https://doi.org/10.1038/s41467-025-62632-x.

**Correspondence** and requests for materials should be addressed to Oscar Palomares.

**Peer review information** *Nature Communications* thanks Julia Eckl-Dorna, Alain Jacquet, and the other, anonymous, reviewer(s) for their contribution to the peer review of this work. A peer review file is available.